Remote Sensing of Environment 224 (2019) 236–258

Contents lists available at ScienceDirect

Remote Sensing of Environment

journal homepage: www.elsevier.com/locate/rse

Wind velocity and wind curl variability over the Black Sea from QuikScat and ASCAT satellite measurements

Arseny Kubryakov*, Sergey Stanichny, Michael Shokurov, Anton Garmashov

Federal State Budget Scientific Institution "Marine Hydrophysical Institute of RAS", str. Kapitanskaya, 2, 2990011 Sevastopol, Russia

A R T I C L E I N F O

Keywords:
Black Sea
Satellite scatterometry
Wind velocity
Wind curl
Topographic effects
Small-scale wind variability

A B S T R A C T

Measurements of QuikScat for 2000–2009 and ASCAT scatterometers for 2009–2016 are used to describe the variability of the Black Sea wind velocity and wind curl. High-resolution (12.5 km) scatterometry data provide a possibility to investigate several small-scale features ("hot points") of the wind field in the basin related to the topographic effects. They include: the gap winds near the Bosphorus, the Kerch Strait, and Tuapse; tip jets at the south and west of the Crimean peninsula, several capes of the Anatolian coast; the Kolkheti valley winds; wind shadow zones at the eastern Turkey coast and the western Crimean coast. Driving factors and directional variability of wind in these "hot points" is discussed.

QuikScat and ASCAT data are used to describe seasonal and interannual variability of wind characteristics in 2000–2016. Comparison with *in-situ* data shows that QuikScat noticeably overestimates wind magnitude during low winds conditions (< 2 m/s). ASCAT winds are generally lower than QuikScat, but the ASCAT wind curl is higher. The amount of low winds values (< 2 m/s) in the ASCAT data is 6% of the total data, and it is 1% in the QuikScat data. Overestimation of low winds decreases wind gradients near the wind shadows, which is the most possible reason of the underestimation of the wind curl in the QuikScat dataset.

Wind curl has a different sign and a completely different interannual variability in the western and eastern parts of the sea. Near the eastern coast of the basin, high-resolution satellite measurements reveal three powerful small-scales maximums of cyclonic vorticity. These maximums are related to the wind jets flowing around topographic obstacles in the vicinity of the Kerch Strait, in the mountain gap near Tuapse, and from the Kolkheti valley. They are observed throughout the whole year, but are largest in winter. The contribution of these maximums to the overall cyclonic vorticity is essential (30% in the QuikScat data and 50% in the ASCAT data). In the western part of the basin, the wind curl is negative (anticyclonic) on average, with the highest anticyclonic curl observed in summer. Winds are decreasing in 2000–2016 in agreement with the data on the 20 century. At the same time the basin-average wind curl rises due to its increase in the eastern Black Sea. We speculate that these trends are associated with the displacement of the Siberian Anticyclone to the west. The related rise of pressure over the eastern Europe correlates significantly with the wind curl variability on interannual time scales.

1. Introduction

Wind stress is the main source of energy for the ocean currents and waves. Wind intensity and direction impact the upwelling dynamics, wind-driven transport of suspended matter and pollutants in the coastal zone, cross-shelf exchange in the basin. Wind stress plays the major role in the modulation of vertical turbulence and mixing, which significantly impacts the thermohaline structure of the Black Sea. Accurate knowledge of wind velocity is crucial for understanding and modeling of wave dynamics, which is in its turn needed for the maritime safety and coastal economy.

Wind curl is another characteristic of high importance for the basin dynamics. Ekman pumping generated by the wind curl is the main factor driving dynamic sea level changes, basin scale and mesoscale Black Sea circulation at seasonal and interannual time scales (Stanev, 1990; Stanev et al., 2000; Korotaev et al., 2001; Kubryakov and Stanichny, 2015a; Kubryakov et al., 2016, 2018). In its turn, basin circulation largely controls nutrient fluxes and, therefore, ecosystem functioning in the basin (Oguz et al., 2002; Zatsepin et al., 2003; Shapiro et al., 2010; Kubryakov et al., 2016).

The largest amount of information about winds dynamics in the Black Sea region was obtained from the coastal meteorological stations

* Corresponding author.
E-mail address: arskubr@ya.ru (A. Kubryakov).

https://doi.org/10.1016/j.rse.2019.01.034
Received 27 April 2018; Received in revised form 18 January 2019; Accepted 28 January 2019

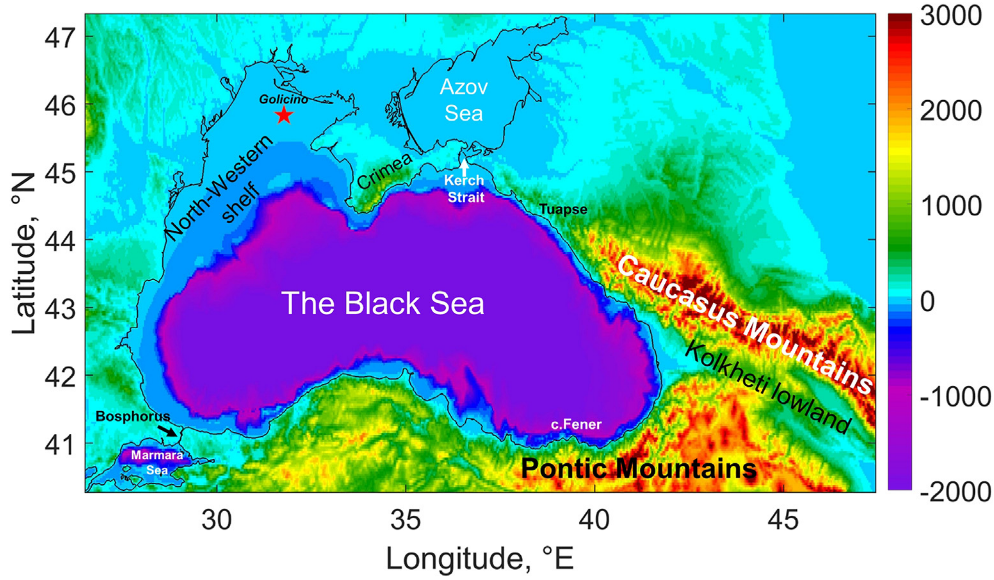

Fig. 1. The Black Sea region orography (m) from ETOPO2v2. Red star shows the position of the Golicino platform. (For interpretation of the references to color in this figure legend, the reader is referred to the web version of this article.)

data and measurements on the research vessels (*e.g.* Sorokina, 1974; Simonov and Altman, 1991). These long-term, continuous measurements provided the first knowledge about large-scale wind variability over the basin and information about wind changes in the region on time scales of several decades.

The large-scale atmospheric circulation is related to the impact of the Siberian Anticyclone in the east (intensifying in winter), the impact of the Azores Anticyclone in the west (intensifying in summer), the Asian low-pressure area, and the low pressure area over Arctic in winter (Arctic oscillation) (Fig. 2). The winds are largely affected by the Black Sea topography (Fig. 1). Higher Caucasus Mountains in the eastern part and lower Pontic Mountains in the southern part of the basin block winds from the east, south and southeast, significantly modifying the Black Sea wind characteristics. The Crimean Peninsula in the north divides the basin in two parts. Relatively low Crimean Mountains affect the low level winds in the northern part of the sea. In summer the domination of the Azores Anticyclone in the western part of the basin leads to the northerly and northeasterly winds. These winds, and additional action of the monsoon effect, induce anticyclonic wind patterns over the western part of the basin (Efimov and Anisimov, 2011a,b). Synoptic variability of the winds in the basin is largely affected by the impact of passing cyclones from the Mediterranean Sea and the northern Europe (Sorokina, 1974; Grishin et al., 1991; Lefevre and Nielsen-Gammon, 1995; Efimov et al., 2009; Yarovaya and Shokurov, 2012).

Modern studies based on the meteostation data provide information about the variability of average and extreme wind velocity and direction in different areas of the basin, its seasonal, long-term variability and climatic trends (*e.g.* Repetin and Belokopytov, 2008, 2009; Garmashov and Polonsky, 2011; Ilyin et al., 2012; Onea and Rusu, 2014). These data show that the wind velocity over the basin has decreased over the last century, leading to the decline of storm severity (Repetin and Belokopytov, 2008, 2009; Ilyin et al., 2012) and wave height in the basin (Arkhipkin et al., 2014). Wind decrease in Belokopytov et al. (2017) is associated with the reduction of a number of propagating atmospheric cyclones over the basin, related to the change of the large-scale atmospheric patterns. The main limitations of the *in-situ* data are the small amount of measurements over the open sea and their irregularity in space, which does not permit to precisely estimate wind curl or divergence, or to understand mesoscale atmospheric variability.

Global and regional atmospheric reanalysis provide the first regular information about spatial variability of the wind and wind curl over the basin (Kara et al., 2005; Kazmin and Zatsepin, 2007; Efimov and Anisimov, 2011a; Valchev et al., 2010; Ivanov and Belokopytov, 2013; Shokurov and Shokurova, 2017; Efimov and Yurovsky, 2017). Several studies demonstrated that modern reanalyses show a good coincidence with *in-situ* measurements and they have reasonable quality for reproducing of the Black Sea wave dynamics in different wave models (Arkhipkin et al., 2014; Divinsky and Kos'yan, 2015; Van Vledder and Akpınar, 2015, Akpinar and de León, 2016; Kubryakov et al., 2016). Seasonal variability of wind characteristics in the Black Sea on the base of the wind reanalysis or regional numerical modeling was investigated in Efimov et al. (2002), Efimov and Anisimov (2011a, 2012), Efimov and Barabanov (2013) and others. Data of atmospheric models demonstrate that local topographic and land-sea interaction effects are very important for the near-surface atmospheric circulation in the enclosed Black Sea (Efimov et al., 2002; Zatsepin et al., 2003; Efimov and Anisimov, 2011a,b, 2012; Efimov and Barabanov, 2013; Shokurov, 2012; Kubryakov et al., 2015; Efimov and Yurovsky, 2017). Particularly, it was shown that the atmospheric circulation over the Black Sea is largely related to the differences in the heat fluxes over the land and sea, *i.e.* monsoon effect. Positive heat flux from the sea in the winter period result in the formation of the cyclonic circulation over the basin, significantly contributing to the overall cyclonic circulation in the 0–1000 m atmospheric layer (Grigoriev and Petrenko, 1999; Korotaev, 2001; Efimov et al., 2002; Efimov and Anisimov, 2011b, 2012). Land-sea temperature differences play an important role in the modulation of winds and wind curl in the coastal areas of the basin on time scales from daily to interannual (Efimov and Anisimov, 2011a,b, 2012; Kubryakov et al., 2015). Topographic effects, particularly wind flow around the Caucasus Mountains, are one of the major factors defining average wind variability in the whole eastern part of the basin (Efimov and Anisimov, 2011a, 2011b; Efimov et al., 2011; Efimov and Yurovsky, 2017).

With the improved resolution, regional reanalysis makes it possible to detect and study the importance of mesoscale atmospheric features in the basin. Several case studies were conducted to investigate a number of mesoscale topographic wind effects: the intense katabatic winds - Novorossiyskaya bora and formation of the Caucasus cyclone over the eastern Black Sea (Efimov et al., 2009; Shokurov, 2012; Efimov and Barabanov, 2013; Yarovaya and Efimov, 2014). Authors of Alpers et al. (2011) and Efimov and Mikhaylova (2017) showed that the interaction of the large–scale circulation with high Caucasus Mountains contributes to the development of mesoscale cyclones over the eastern Black Sea. Automated eddy-identification methods were used to quantify and investigate the properties of the Black Sea mesocyclones on the base of > 30-year data (Efimov et al., 2009; Yarovaya and Shokurov, 2012; Yarovaya, 2016).

Although resolution of modern atmospheric reanalysis is rather high, the complexity of the atmospheric processes makes it difficult to reproduce correctly all the features of wind characteristics, especially in the costal zones, near the topographic or orographic obstacles (Accadia et al., 2007). Satellite scatterometers provide measurement-based information about wind variability with high resolution (12.5 km). These high-resolution data allowed us, for the first time, to understand a large number of small-scale processes in the world atmosphere, such as the impact of sea temperature gradients on the wind divergence and curl variability (Chelton et al., 2004; Risien and Chelton, 2008), the significant impact of tip jets and corner winds on the thermohaline structure of the ocean (Moore and Renfrew, 2005), climatic patterns of wind on small spatial scales (Desbiolles et al., 2017).

In the Black Sea, the data of the QuikScat scatterometer for 2000–2009 were used to study the distribution and time variability of extreme winds in Chronis et al. (2011). Zecchetto and De Biasio (2007) investigated the winds characteristics over the Mediterranean basin in 2000–2004 from the QuikScat data. Authors provided data on the seasonal variability of wind velocity and wind curl over the Black Sea. They demonstrated significant differences in wind curl in the eastern and western parts of the basin, which was attributed to the impact of orographic effects. Satellite scatterometry was used to study episodic extreme events in the Black Sea atmosphere: the powerful quasi-tropical cyclone (Efimov et al., 2007, 2008) and extreme storms in Shokurov (2012). In Kubryakov et al. (2015) authors used the QuikScat data for 2000–2009 to investigate interannual variability of coastal winds and its relation to the land-sea temperature contrasts.

The scatterometry winds were used as forcing for the circulation and wave models. The validation on the base of *in-situ* data in these studies has showed that the use of satellite data is preferable to atmospheric models (Kara et al., 2005; Van Vledder and Akpınar, 2015). Another source of high-resolution satellite information about the Black Sea wind variability is synthetic aperture radars (SAR) data. SAR measurements were used to document and study valley (foehn) wind in the south-eastern part of the basin in Kolkheti Lowland and its interaction with an atmospheric cyclonic eddy (Pustovoitenko and Malinovsky, 1998; Alpers et al., 2011), Novorossiyskaya bora (Alpers et al., 2009). These studies demonstrate the development of the strong jet from Kolkheti Lowland, which can reach velocities of 30 m/s, significantly impacting the wind variability in the south-eastern part of the sea.

In our study we use the data of QuikScat and ASCAT-A, B for > 15 years (2000–2016) to study the spatial and temporal variability of the wind velocity and wind curl over the Black Sea. Particular attention is paid to the investigation of small-scale wind topographic effects, such as gap winds, tip jets, valley winds, which are well seen in satellite data and are shown to significantly impact the wind characteristics in the basin. The manuscript structure is as follows. The data are described in Section 2. Validation of the scatterometry data on the base of comparison with *in-situ* measurements on the offshore platform, and intercomparison of the ASCAT and QuikScat data is given in Section 3. Spatial variability of the wind velocity is analyzed in Section 4. Small-scale features of the wind variability and their causes are discussed in Section 5. Seasonal and interannual variability of wind velocity is studied in Section 6. Spatial, seasonal and interannual variability of the wind curl is analyzed in Section 7. In Section 8 we discuss the relation of the large-scale atmosphere circulation with the wind variability in the basin (Section 8.1) and the impact of the wind forcing on the Black Sea dynamics (Section 8.2). Conclusive remarks are given in Section 9.

2. Data

2.1. Satellite scatterometry

In this study we use Level 2 data of wind vectors derived from the measurements of QuikScat scatterometers for 2000–2009, ASCAT A for 2009–2016 and ASCAT B for 2012–2016. Scatterometers measure the ocean surface radar backscattering σ0, related to the magnitude of capillary waves, on different frequencies and polarizations. These measurements enable the computation of the wind direction and magnitude using empirical geophysical model function.

We use Level 2B array of QuikScat data provided on a non-uniform grid within the swath at 12.5 km pixel resolution (https://podaac.jpl.nasa.gov/dataset/QSCAT_LEVEL_2B_OWV_COMP_12) (Fore et al., 2014). The 12.5 km binning resolution enables users to obtain wind vector retrievals 10 km closer to the shore when compared to the 25 km L2B dataset. The QuikScat data over the Black Sea are available approximately twice per day (between 01:00–04:00 and 13:00–17:00 UTC).

We also use the MetOp ASCAT Level 2 Ocean Surface Wind Vectors Optimized for Coastal Ocean product (KNMI 2010, https://podaac.jpl.nasa.gov/dataset/ASCATA-L2-Coastal). This dataset contains operational near-real-time Level 2 coastal ocean surface wind vector retrievals from the Advanced Scatterometer (ASCAT) on MetOp-A and MetOp-B with 12.5 km sampling resolution. It is a product of the European Organization for the Exploitation of Meteorological Satellites (EUMETSAT) Ocean and Sea Ice Satellite Application Facility (OSI SAF) provided through the Royal Netherlands Meteorological Institute (KNMI). This coastal dataset differs from the standard 12.5 and 25 km datasets in that it utilizes a spatial box filter (rather than the Hamming filter) to generate a spatial average of the σ0 retrievals from the Level 1B dataset. All full resolution σ0 retrievals within a 15-km radius of the wind vector cell centroid are used in the averaging. With this enhanced coastal retrieval, winds can be computed as close to ~15 km from the coast, as compared to the static ~35 km land mask in the standard 12.5 km dataset (Verhoef and Stoffelen, 2013). ASCAT-A and ASCAT-B measure over the Black Sea at 06:00–09:00 UTC and 17:00–20:00 UTC. The ASCAT-L2-Coastal dataset has been available since August 2010. We use this dataset in the period from 2011-01 to 2016-01. As rain drops can significantly change radar backscattering, the scatterometry data with "rain" flag were excluded from the analysis.

To obtain wind characteristics from the ASCAT-A in 2009–2010, we use operational near-real-time Level 2 ocean surface wind vector retrievals from the Advanced Scatterometer on MetOp-A with 12.5-km sampling resolution (https://podaac.jpl.nasa.gov/dataset/ASCATA-L2-12.5km) (Verspeek et al., 2009). This product is not available in the coastal zone at ~35 km from the coast. The combined dataset consisting of ASCAT Level 2 in 2009–2010 and ASCAT-L2-Coastal in 2011–2016 was used for the analysis of the winds time variability in 2009–2016. For the analysis, satellite data are binned on a regular grid with the 12.5-km resolution.

Wind curl W is computed from data on regular grid as $W = \frac{dv}{dx} - \frac{du}{dy}$, wind magnitude V is computed as $V = \sqrt{u^2 + v^2}$, where u,v are zonal and meridional wind component. Wind curl and velocity are then daily averaged to obtain daily dataset of wind characteristics.

2.2. Era-Interim reanalysis

Wind velocity at 10 m height and Sea Level Pressure (SLP) for 1979–2016 from the ERA-Interim reanalysis are used in this study. ERA-Interim is a global atmospheric reanalysis that is produced by the European Centre for Medium-Range Weather Forecasts (ECMWF) (Dee et al., 2011). The spatial resolution of the array is 0.75° × 0.75°, and the temporal resolution is 6 h.

2.3. In-situ measurements

For the validation purpose, we use wind measurements on the offshore gas platform "Golicino-4". The platform is situated > 60 km away from the coast in the north-western part of the basin (31.88°E, 45.71°N) (see Fig. 1). An M63MP sensor measuring magnitude and direction of wind was mounted on the highest point of the platform at the height of 37 m above sea level. Wind characteristics were obtained by averaging measurements in 10 min intervals. Data are available with 3-h discretion in 1996–2002 and with 1-h discretion in 2008–2009. Detailed information about meteorological complex and data processing can be found in Toloknov et al. (1998) and Garmashov and Polonsky (2011). Data in 2000–2002 and 2008–2009, totally > 7800 measurements, were used for the comparison with the QuikScat data. Wind data are adjusted to a standard height of 10 m according to the Monin–Obukhov theory (Monin and Obukhov, 1954) (see details in Garmashov et al., 2016). Unfortunately, *in-situ* data were not available after 2009, which is why the validation is done only for the QuikScat data.

3. Assessment of scatterometers accuracy

3.1. Validation of QuikScat winds with in-situ data

For the comparison, we chose the nearest measurements of QuikScat scatterometry and *in-situ* data within a 1-h time interval and a 10-km distance interval. Totally 1480 pairs of measurements were selected. The scatter diagram of wind magnitude between satellite and *in-situ* data is shown in Fig. 3a. The regression coefficient is 0.98, correlation coefficient is 0.85, estimated standard deviation is 1.53 m/s. Bias, defined as average difference between *in-situ* and QuikScat wind magnitude, is −0.17 m/s. The average error of 1.58 m/s is somewhat higher than the error obtained from the global validation of ~1 m/s (Ebuchi et al., 2002).

The accuracy of the QuikScat data depends on the wind magnitude. Average relation between QuikScat and *in-situ* measured wind magnitude (black line in Fig. 3a) shows that QuikScat data overestimates weak winds in the intervals of 0–2 m/s. QuikScat data in this interval is on average 0.5–1.5 m/s higher. The error of direction estimates is also significantly larger for low winds. It decreases from 40 to 60° for wind speed of 1–3 m/s to only about 15–10° for the wind speed higher than 5 m/s (Fig. 3b) in agreement with (Bentamy et al., 2008). During low winds the backscattering from capillary waves is weak, and the contribution of instrumental noise increases. Limitation of the device sensitivity leads to the rise of errors during low winds known from the previous studies (Ebuchi et al., 2002; Bentamy et al., 2008, 2012). In strong wind conditions, QuikScat slightly underestimates wind magnitude. For the wind velocity V > 10 m/s, average bias is about 0.5–1 m/s (Fig. 3a). Contribution of whitecaps, air spray and other complex processes observed during storm winds complicates the description of the GMF function describing the relation between the ocean surface radar backscattering and wind velocity (Ebuchi et al., 2002).

3.2. Intercomparison of ASCAT and QuikScat winds

ASCAT and QuikScat winds have previously been compared in Bentamy et al. (2008, 2012). Authors showed that the ASCAT winds are higher than the QuikScat retrievals for low winds (V < 5 m/s) and lower than the QuikScat retrievals for high winds (V > 10 m/s). In Bentamy et al. (2012) some of these inconsistencies were explained by impact of rain rate and SST. Here, we provide a short comparison of ASCAT and QuikScat in the Black Sea region in terms of wind velocity and curl to understand the possible uncertainty in the obtained regional wind characteristics.

Wind data in April–November 2009 were used. For the comparison, collocated QuikScat and ASCAT measurements within 20-km and 3-hour distance were chosen. Totally, > 190,000 collocated measurements were obtained.

A graph of monthly-averaged wind velocity from the collocated array (Fig. 3c) shows that the QuikScat winds are on average 0.5 m/s higher than the ASCAT winds. The largest differences (0.5–0.7 m/s) are observed in summer (June–August) and lesser differences – in spring and autumn (0.3–0.4 m/s).

The histogram of wind velocities and differences between the data amount in different intervals of wind velocity are shown in Fig. 3d and e. One bar in these graphs corresponds to a 1-m/s bin. It is seen that the amount of low wind velocities (W < 2 m/s) in the QuikScat dataset is significantly lower than in the ASCAT array in agreement with (Bentamy et al., 2008). The total amount of such low wind velocities is ~ 6% in the ASCAT data and ~1% in the QuikScat data. Accuracy of scatterometers is insufficient during weak winds (see *e.g.* Ebuchi et al., 2002; Bentamy et al., 2012). The shape of the tail of the GMF function should primarily impact this statistical distribution during such low wind velocities. Close analysis of the histogram for low winds (not shown) demonstrates that the amount of wind values decreases rapidly between 2 m/s and 0 m/s in the QuikScat dataset, while it is almost constant for all values in 0–2 m/s in the ASCAT dataset. The same issue – small number of realizations of wind speed under 2 m/s was noticed by the developers of the KNMI scatterometry products for QuikScat (Stoffelen et al., 2001). They suggest that "this phenomenon is probably related to the inversion scheme and requires further study".

At the same time the QuikScat dataset contains more values than the ASCAT for moderate wind velocities in 3–11 m/s interval (Fig. 3d,e). The largest differences are observed for sufficiently strong winds V = 7–11 m/s (Fig. 3e). The contribution of wind velocities in this interval to the total difference between the QuikScat and the ASCAT data can be computed by multiplying the difference of data amount in Fig. 3g by the corresponding value of wind velocity. This exercise shows that the higher amount of winds in 7–11 m/s in the QuikScat data can explain 78% of the observed negative difference between the ASCAT and the QuikScat wind magnitudes.

At the same time the amount of strongest winds (V > 12 m/s) is less in the QuikScat data in agreement with (Bentamy et al., 2008). Generally, the QuikScat array contains more moderate winds (V = 3–12 m/s), while the ASCAT array contains more peak minimal and maximal values. Therefore, the distribution of the QuikScat winds is statistically smoother than that for the ASCAT winds. This should result in underestimation of the wind gradients and curl in the QuikScat data. To demonstrate this, the average relation between the ASCAT wind velocity and the ASCAT wind curl is shown in Fig. 3f. The highest wind curl corresponds to low winds (V = 3–5 m/s) and high winds (V > 13 m/s), which are often associated with strong wind gradients. Minimal wind values are often observed in the zone of wind shadows. As it will be shown further (Section 7), gradients of wind between jet winds and wind shadows related to the topographic effects impact significantly the wind curl in the Black Sea basin.

The diagram showing the differences between the QuikScat and the ASCAT data amount for different intervals of absolute wind curl is shown in Fig. 3g. This distribution demonstrates that the QuikScat data have significantly higher amount of low wind curl values ($W < 4*10^{-5}$ 1/s) and lower amount of high wind curl values ($W > 4*10^{-5}$ 1/s). The amount of weak winds is significantly higher than that of strong winds (see histogram in Fig. 3e). That is why, the overestimation of low winds in the QuikScat dataset is, probably, the major reason of the observed low values of the wind curl.

Concluding above, generally the QuikScat array contains more moderate winds and is smoother than the ASCAT array. This results into lower values of the wind curl in the QuikScat data. At the same time winds in the QuikScat array are higher due to a larger amount of relatively strong winds in the 7–11 m/s interval. These differences should be taken into account while interpreting the results of the present investigation.

Despite several inconsistencies during high and low winds, satellite

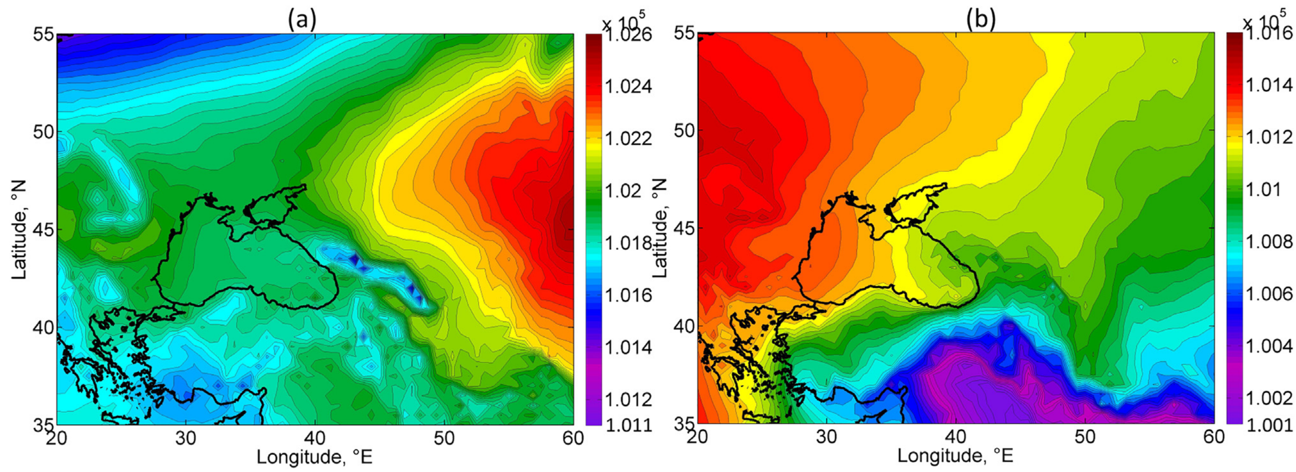

Fig. 2. Pressure distribution at sea level (SLP, Pa) from the Era-Interim reanalysis averaged over winter (a), when the action of the Siberian Anticyclone was prevailing, and over summer (b), when the action of the Azores Anticyclone was prevailing for 1980–2016.

scatterometry data give the most accurate information on the wind magnitude and direction, as obtained statistical characteristics for the QuikScat data are better than those for the modern atmospheric reanalysis in the Black Sea (Garmashov et al., 2016).

4. Spatial variability of wind velocity characteristics

Maps of time-averaged winds, computed by averaging wind vectors in time, and wind magnitudes from QuikScat for 2000–2009 and ASCAT for 2009–2015 are shown in Fig. 4a–d. Spatial distribution of wind characteristics from the QuikScat and the ASCAT data is similar. Some observed differences are related both to the long-term trends of wind velocity and dataset processing.

Average winds over the basin are directed southward, that is related to the action of the Azores Anticyclone in the warm period of a year and the Siberian Anticyclone in winter (Fig. 2). Winds are directed on average southwestward in the western part of the sea, and southeastward in the eastern part (Fig. 4a,b). In the warm period of the year the Black Sea is situated on the eastern periphery of the Azores Anticyclone (Fig. 2b), which results into prevailing north-northwesterly winds. Blocked by the Pontic Mountains, they turn to the east on eastern side and to the west on western side of the sea (Efimov et al., 2002). In winter the Black Sea large-scale wind variability is related to the action of the Siberian Anticyclone in the east (Fig. 2a). Easterly and southeasterly winds from the continent are blocked on the east by the high Caucasus Mountains. Large-scale winds flow around the Caucasus Mountains inducing strongest north-northeasterly winds over the Black Sea.

Wind magnitudes (Fig. 4c,d) on average are higher in the northeastern and southwestern (5.5–7 m/s) parts of the basin, which is related to the action of strong northeasterly winds in winter. The minimum of the wind velocity is situated in the southeast due to the blockage by surrounding mountains. Wind magnitude over the Sea of Azov is higher than over the Black Sea (~6–7 m/s). The Sea of Azov surrounded by flat relief is directly impacted by the most intense winds associated with the action of the Siberian Anticyclone in the cold period. These features of the Black Sea wind characteristics are well-known from the previous climatic and model studies (*e.g.* Sorokina, 1974; Efimov et al., 2002; Zechetto et al., 2007; Efimov and Anisimov, 2011a, 2012; Efimov and Barabanov, 2013).

Prominent minimum of wind velocity (L1, Fig. 4c,d) is observed in the southwestern part of the Black Sea in the box (30–32°E, 41–42.5°N). In the central southern part of the Black Sea land extends to the sea for ~100 km and divides the Black Sea into two parts. The Pontic Mountains in this part with the height of ~1000–1500 m form a topographic barrier for the easterly and northeasterly winds prevailing in winter, which results in the formation of the wind shadow zone in this area (Zechetto et al., 2007). Another small minimum zone of wind magnitude (L2) is observed near the southeastern coast of Crimea. The Crimean Mountains with the height of ~1000 m in this area block northerly, northeasterly and northwesterly winds (Efimov and Anisimov, 2011a; Efimov and Barabanov, 2013; Efimov and Komarovskaya, 2015), which results in the local wind shadow zone with minimum of wind velocity in the box (35–36°E, 44–45°N).

High-resolution satellite scatterometry reveals several "hot spots" - local maximums of wind magnitude in the Black Sea (Fig. 4d): very local maximum (H1) near the Bosphorus; the strongest maximum H2 – to the south of the Kerch Strait; maximums H3 and H4 – to the south and west of the southwestern Crimean peninsula near Sevastopol; H5 - off the central western Black Sea coast.

Maps of standard deviations (*std*) of wind magnitude show several additional features of the Black Sea wind circulation characterized by an increased wind magnitude variability (Fig. 4e,f). The largest variability is observed in the northeastern and northern parts of the sea off the Crimean eastern coast (S1 – Fig. 4e). The combination of several effects: strong winds blowing through the Kerch Strait, cape effect near Sevastopol (see Section 5), the Crimean Bora (wind blocked by the Crimean Mountains) seems to play an important role in the formation of this maximum (Efimov and Barabanov, 2013; Efimov and Komarovskaya, 2015). Another large maximum of *std* is detected off the western coast of the basin (S6). The possible reason of an increased variability in this area, characterized by relatively flat topography, is the monsoon and breeze winds (Efimov and Anisimov, 2011b, 2012). The Sea of Azov is also characterized by increased values of *std*.

Several very local small-scale maximums of wind variability (*std*) are observed in Fig. 4e,f. The maximum S2 in the northwestern part is located near Tuapse with the center point at 39°E, 44°N. Maximum S3 is located in the southeastern (centered at 41°E, 42°N) area off the entrance of the Kolkheti Lowland. A less intense maximum S4 is located on the southern coast in the southeast at (39.5°E, 41.5°N) near the cape Fener in the vicinity of the city of Trabzon. S5 is observed off the southern central part of the basin. Let us discuss the wind variability in these local maximums in more detail.

5. Small-scale "hot spots" of the Black Sea wind variability

The QuikScat data was used to choose the wind data in the local areas of maximum wind magnitudes (H1–H5 – Fig. 4d) and variability (S2–S5 – Fig. 4e). To understand the reasons of the increased winds and their variability in these points, we compute the wind roses in the

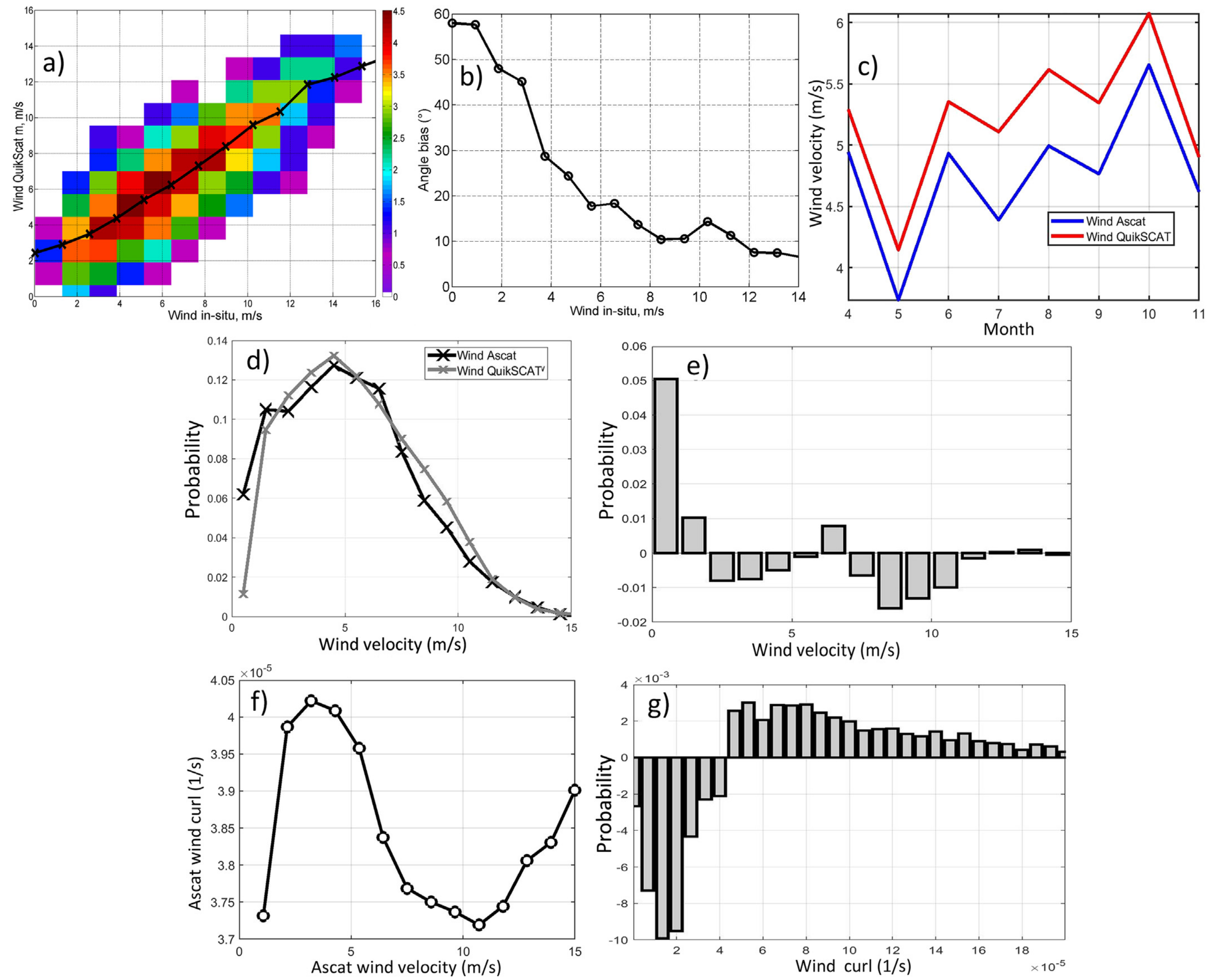

Fig. 3. a) Scatter diagram between *in-situ* and QuikScat wind magnitude (m/s). Black line shows average relation between two datasets. Colors show the number of points in each bin. b) Dependence of the absolute error of wind direction (°) on the *in-situ* wind magnitude (m/s); c) comparison of monthly-averaged QuikScat and ASCAT collocated data; d) histogram of wind magnitudes of QuikScat and ASCAT data; e) difference of data amount between the ASCAT and the QuikScat datasets in different intervals of wind magnitude; f) average dependence of ASCAT wind curl on wind velocity; g) difference of data amount between the ASCAT and the QuikScat datasets in different intervals of absolute wind curl. (For interpretation of the references to color in this figure legend, the reader is referred to the web version of this article.)

center of these areas for the winds > 8 m/s (Fig. 5). The wind roses are plotted in oceanographic projections, *i.e.* they show the direction in which winds blow. Fig. 6 shows several instantaneous maps of wind velocity with examples of small-scale wind processes. Additionally, we choose the situations with the strongest winds in these points (magnitude exceeds 95 percentile) and calculate average maps of wind magnitudes for these situations, to which we will refer later as composite maps (Fig. 7).

Near the Bosphorus (H1) the very local maximum is observed almost throughout the whole year. The spatial scale of wind maximum, estimated visually on the base of Fig. 4d, is only about 20 km. This maximum is probably related to the gap winds in the strait. The pressure gradient between the Black and the Marmara Seas orients along the channel and wind streamlines converge in the gap. This results into the increase of wind in the strait and 10–20 km to the north of the strait entrance when southwesterly winds blow from the Marmara Sea to the Black Sea. Such winds are detected in this point in autumn and winter, however their frequency is not high. The instantaneous map showing the example of strong southerly storm wind on 26 November 2007 with maximum velocity near the Bosphorus is shown in Fig. 6a. However, more frequently the intense winds in this point are observed during northeasterly storms (Fig. 6b–d), that are typical for the Black Sea. Composite maps of wind intensity for the wind maximums in this area (Fig. 7a) show that the largest wind intensity is observed here during strong southerly winds blowing in the western part of the basin. Superposition of the local maximum due to gap winds and regular storm northeasterly winds additionally increases wind magnitude in this zone forming a “hot-spot” of wind intensity.

The increase of wind velocities near the Kerch Strait (H2) was mentioned earlier in a number of studies (Repetin and Belokopytov, 2008; Ilyin et al., 2012). This maximum is probably related to the relatively large gap (flat relief) situated between the Crimean Mountains to the west and the Caucasus Mountains to the east. The topography of the Kerch and the Taman Peninsulas is almost flat, and strong northeasterly winds penetrate in the area between 35.3°E and 37.4°E. Local maximum here is relatively large; on average, it extends to 50 km

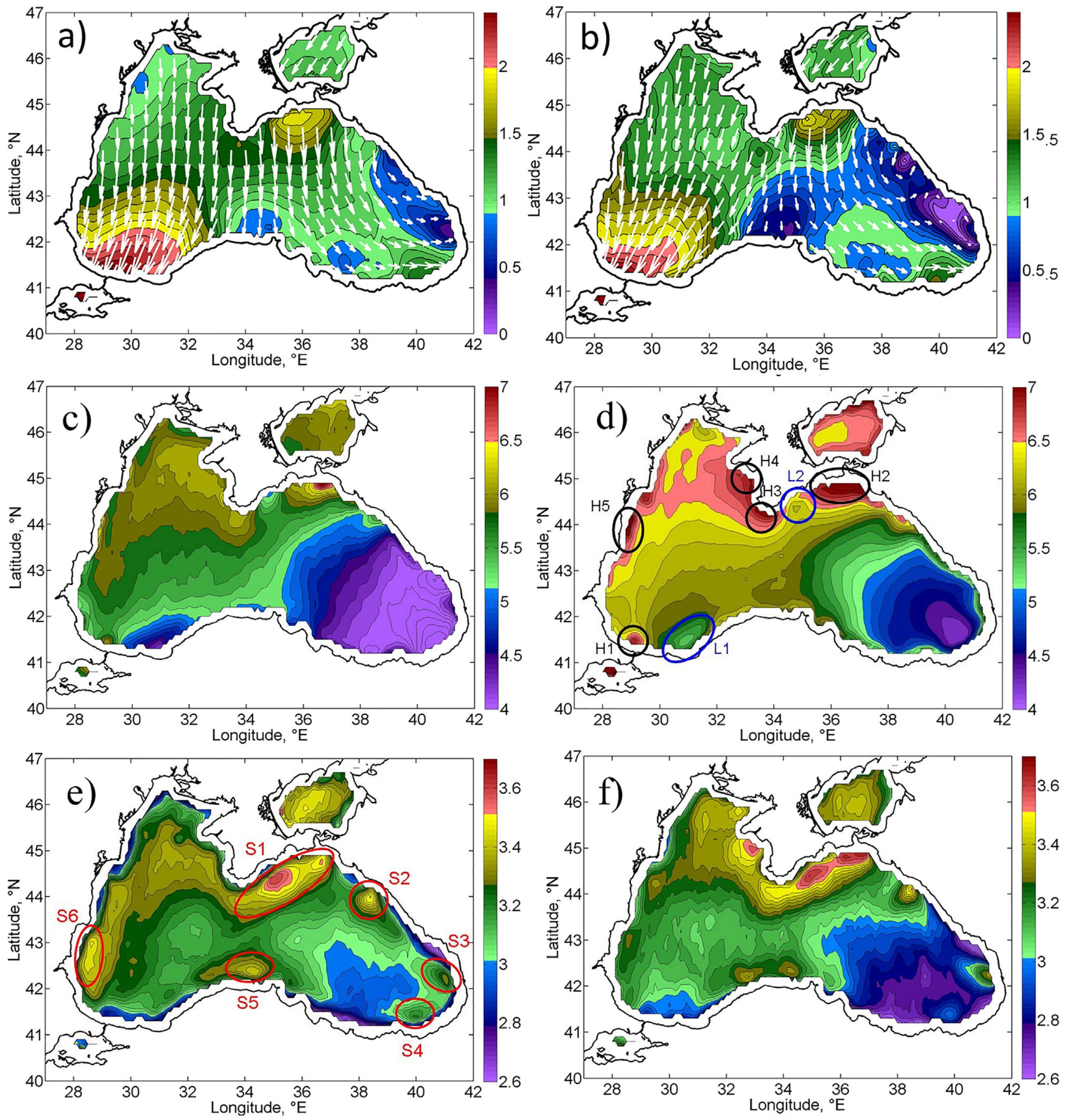

Fig. 4. a, b) Average wind velocity (m/s) from the QuikScat data for 2000–2009 (a) and the ASCAT data for 2009–2015 (b). Scales of arrows are shown by color; c, d) average wind magnitude (m/s) from the QuikScat data for 2000–2009 (c) and from the ASCAT data for 2009–2015 (d); e, f) map of standard deviation of wind magnitude (m/s) from the QuikScat (e) and the ASCAT (f) data. (For interpretation of the references to color in this figure legend, the reader is referred to the web version of this article.)

offshore and covers the entire shelf zone near the Kerch Strait. Large winds in this shelf zone are one of major reason of the intense transport of Azov waters in the Black Sea and resuspension of bottom sediments (Goryachkin et al., 2005; Shcherbak et al., 2008; Aleskerova et al., 2017). The wind rose plotted in Fig. 5b shows that the highest winds here are associated mostly with northeasterly winds, which are related, primarily, to the action of the Siberian Anticyclone in the cold period of a year.

The instantaneous wind maps for 15 December 2010 and 10 November 2008 show examples of local intensification of wind in this area (Fig. 6b,c). Northeasterly winds significantly intensify after passing the Kerch Strait. Local maximum of wind intensity extends up to the southern Crimean coast in the southwest direction. Composite maps in Fig. 7b demonstrate a similar distribution of wind magnitudes. Local maximum is elongated in the southwestern direction at a distance of 100–200 km from the strait. Typically during such storms the local maximums of wind magnitude are also formed off western Crimea and at the northeastern Black Sea coast, near Tuapse (see example in Fig. 6b).

Two close maximums H3 and H4 are observed to the southwest and west of Crimea. The wind rose for strong winds in the maximum H3 located near the southern point of Crimea, cape Sarych, shows two

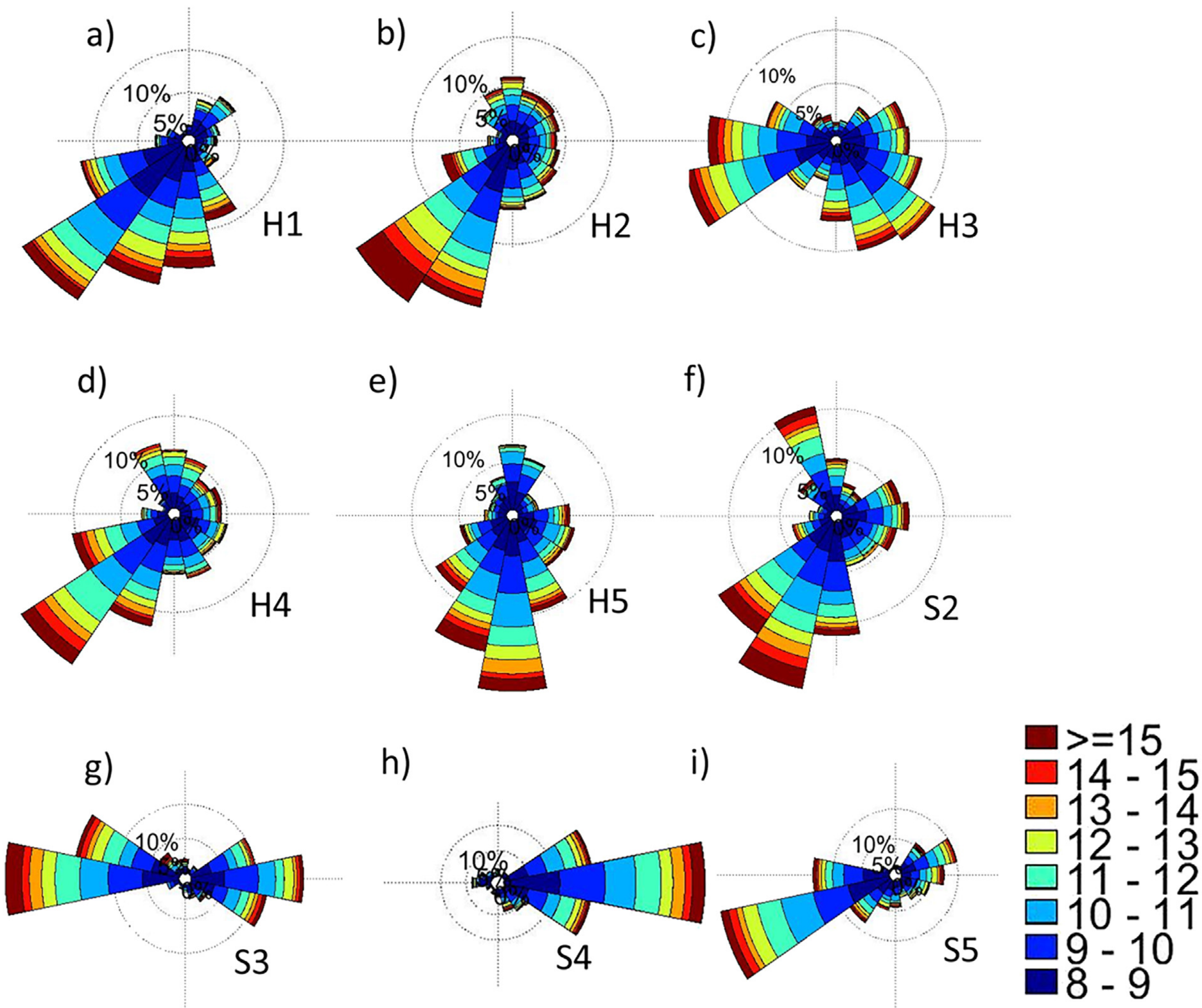

Fig. 5. Wind roses in oceanographic projection for the center of the following areas: a) H1 – near the Bosphorus (29.1°E, 41.5°N); b) H2 (36.8°E, 44.85°N) – the Kerch Strait; c) H3 (33.6°E, 44.25°N) – southwestern Crimea; d) H4 (33.2°E, 44.9°N) – western Crimea; e) H5 – the western Black Sea coast (29°E, 44.05°N); f) S2 – Tuapse (38.5°E, 44.1°N); g) S3 – the Kolkheti Lowland (41.2°E, 42.25°N); h) S4 – cape Fener (39.8°E, 41.4°N); i) S5 – the southern central coast (32.7°E, 42.2°N). Colors show the magnitudes of the wind velocity (see color legend in the right bottom corner). (For interpretation of the references to color in this figure legend, the reader is referred to the web version of this article.)

general directions – easterly and northwesterly (Fig. 5c). The examples of situations with local wind maximums in this zone for both directions are given in Fig. 6d,e,f,g. It is clearly seen that in all of the examples wind increases on the leeward side of the cape and then turns to the coast. The strongest local maximum is formed near southern Crimea and the increase of wind is observed at the distance of 50–200 km from the cape. This increase is related to the tip winds generated due to the effect of the topographic obstacle on the cape (Moore and Renfrew, 2005). Mountains partially block the winds and the zone of low pressure is formed behind them. The increase in pressure difference near the cape results into rapid intensification and rotation of the easterly or southeasterly winds to the northeast-north behind the topographic obstacle, while northwesterly winds rotate to the east. The composite analysis in Fig. 7c shows that the area of the most intense winds is observed to the southwest of southern Crimea.

The zone of the winds intensification in this area is determined by the direction of inflowing winds. When the winds flow from the south, the maximum is formed off the western Crimean coast H4 (Fig. 6f). Such winds significantly impact the suspended matter transport in this area, causing large damage of beaches infrastructure (Kosyan et al., 2012; Aleskerova et al., 2015). The wind rose (Fig. 5d) and the composite map (Fig. 7d) for maximum H4 show that the storm northeasterly winds are also of significant importance for the local wind increase. The winds from this direction, observed mostly in winter, are partly blocked by the Crimean Mountains. The low pressure area formed behind the mountains causes the local intensification of winds. A band of higher wind velocities is observed at the distance of 50 km offshore over the whole western shelf of Crimea.

Maximum H5 is located near the west coastline of the Black Sea. In this area the relief is relatively flat. The monsoon and breeze winds are the possible reasons for the increased coastal winds intensity and variability (Efimov and Anisimov, 2011a,b; Kubryakov et al., 2015). The average wind velocity in this area depends on the value of the land-sea temperature contrasts on seasonal and interannual time scales (Kubryakov et al., 2015). In winter land-sea temperature contrasts over this flat region are strong, that induces intense southward alongshore winds. The strongest winds are usually observed in the vicinity of the coastal zone at 42°–45°N (Fig. 7e). The effect of the monsoon winds in winter is clearly seen on the seasonally-averaged wind maps (see Fig. 9a, Section 6). The highest winds in this area are observed mostly during northerly winds, and less-frequently during southerly winds (Fig. 5e).

The intense and local maximum of wind variability S2 is observed at the northeastern part. The local relief lowering is observed in this part

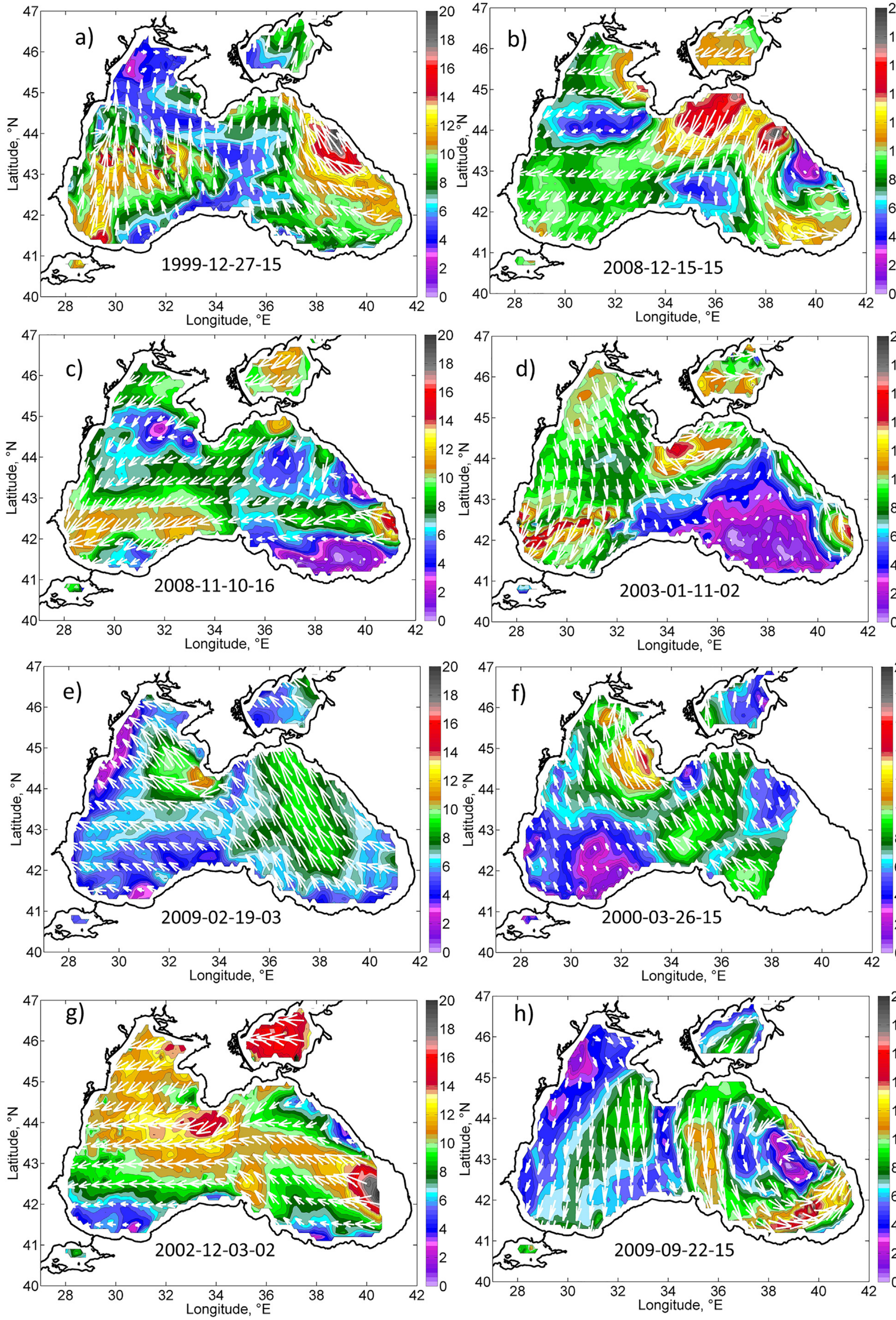

(caption on next page)

Fig. 6. Examples of instantaneous wind maps from the QuikScat data showing the formation of local maximums of wind velocity for: a) 27 December 1999; b) 15 December 2008; c) 10 November 2008; d) 11 January 2003; e) 19 February 2009; f) 26 March 2000; g) 3 December 2002; h) 22 September 2009. Colorbar shows wind magnitude (m/s). Note different color scale limits. (For interpretation of the references to color in this figure legend, the reader is referred to the web version of this article.)

of the Caucasus Mountains. When cold dense air deepens sufficiently on the windward side of a barrier, it passes over the crest and then accelerates down the lee slopes. Such katabatic winds, called Novorossiyskaya bora, were extensively investigated (*e.g.* Gusev, 1959; Alpers et al., 2009; Efimov et al., 2009; Efimov and Barabanov, 2013). Cold air overflows mountain ridge here forming a strong cold downslope wind. The difference in pressure on the different sides of the Caucasus Mountains (gap effect) and baroclinicity effects (Bora) contributes to the intensity of jets flowing from the local gap in the mountains to the sea. The wind rose in Fig. 5f and composite maps in Fig. 7f show that the most intense storms in this area are associated with the northeasterly winds. The examples of local wind increase in this area are shown in Fig. 6b,c. These events are often associated with strong northeasterly storms observed over the whole Black Sea, which are related to the pressure difference between the warm Black Sea and the cold land to the east of the Caucasus. The Novorossiyskaya bora and generally northeasterly winds in this area occasionally induce the formation of the mesoscale Caucasus cyclone (Efimov et al., 2009; Shokurov, 2012; Efimov and Mikhaylova, 2017) occupying the south-eastern Black Sea, which is observed in Fig. 6b.

Storm activity in the area S2 is also partly related to the south-easterly winds in winter (Fig. 5f). These winds are associated with the strong atmospheric cyclones that are occasionally formed over the whole eastern part of the Black Sea. The example of such cyclone is given in Fig. 6h. When the strong northerly winds blow over the eastern part of the basin, they are blocked in the southeast by the eastern Pontic Mountains. Northerly winds rotate to the east in the area of low pressure behind Caucasus Mountains to the east and form an atmospheric cyclone. Southerly winds on the right periphery of these cyclones induce southeasterly storms along the whole eastern coast.

Also southeasterly winds in area S2 can be related to the action of valley (or foehn) winds from the Kolkheti Lowland (Burman, 1969), which are the reason for another pronounced maximum S3 of the wind variability (Fig. 4e) in the southeastern part of the sea (41°E, 42°N). The Kolkheti valley is situated between the Greater Caucasus in the north and the Lesser Caucasus in the south and connects the Caspian and the Black Seas. Cold air flows down the slopes and collects in the valley (Pustovoitenko and Malinovsky, 1998; Alpers et al., 2011). The net cooling of the air results in a pressure increase in the valley, which becomes large enough to drive the circulation along the valley axis from the valley to the warm sea. The examples of the intense Kolkheti jet are shown in Fig. 6c,d,g. It is seen than these valley winds can be easterly or southwesterly and can be significantly different in their extent and intensity. Occasionally (see an example in Fig. 6g) the Kolkheti jet can reach 34°N, *i.e.* penetrate 600 km into the center of the Black Sea. Such strong winds significantly impact the wind curl over the basin (Section 7). The composite map in Fig. 7g shows that the strongest Kolkheti valley winds are southeasterly. Westerly winds in this area may also cause storms - Fig. 5g. These westerly winds are related to the formation of an atmospheric cyclone over the eastern Black Sea, discussed in the previous paragraph (see an example in Fig. 6h).

A less intense local maximum of wind variability S4 is located off the southern coast in the southeast of the basin at (39.5°E, 41.5°N). Visual analysis of the wind maps shows that this maximum is related to the tip jets off the cape Fener near Trabzon. The examples of the wind increase during strong atmospheric cyclone in the eastern Black Sea on 15 December 2008 are shown in Fig. 6h. The air flow around the Pontic Mountains on the cape induces the increase of wind on its leeward side, similar to the discussed above tip jets near southern Crimea. Strong winds are observed here only during the wind flow from the west (Fig. 5h), related to the cyclonic winds over the eastern part of the Black Sea (as in the example in Fig. 6h).

The last discussed maximum of *std* S5 is observed off the southern central coast of the basin. In the ASCAT dataset this maximum is divided into two local maximums. The formation of these maximums is also associated with several capes in the southern part of the basin. Anatolian mountainous coast extends in this area to ~100 km in the sea. Northeasterly and northwesterly winds blocked by the mountains in the south flow around the capes on the Anatolian coast (Fig. 5i). This results in the formation of the tip east and west jets on the leeward side of the capes and increase in wind velocity in this area. Composite analysis shows that during the strongest wind in this area winds are also intense to the northwest of the cape, This suggest that northwesterly winds, which flow around the cape, are the most probable reason of the observed maximum S5 (Fig. 7i).

6. Time variability of wind velocity

The seasonal and interannual variability of the basin-averaged wind velocity (Fig. 8a,b, black line – the QuikScat data; blue line – the ASCAT data) shows that the ASCAT winds are generally lower than the QuikScat winds, especially during low winds (< 4 m/s). These differences are especially large in summer, when they exceed 1 m/s (Fig. 8a). The basin-averaged ASCAT winds in the summers of 2009–2015 are lower than 4 m/s, while the QuikScat winds in summer of 2000–2009 are in the interval of 4–5 m/s. Both different processing of the QuikScat and the ASCAT data and long-term decreasing trend of wind velocity is the reason of this discrepancy. These inconsistencies are related mostly to the larger amount of sufficiently strong winds (V = 7–11 m/s) in the QuikScat L2b dataset (see Section 3.2). The overestimation of the winds by the QuikScat in comparison to the ASCAT data was also obtained previously in Bentamy et al. (2008, 2012).

Both datasets show the weak decreasing trend of wind velocity (Fig. 8b). The QuikScat winds fall down by ~0.02 m/s per year from average values of 5.5 m/s in 2000 to 5.3 in 2009. The ASCAT winds decrease by 0.025 m/s from 5.2 to 5 m/s in 2010–2015. We note that the available period of the ASCAT data (6 years) is too short to obtain the significant trend values, and the given estimates can be regarded only as approximate. The interannual variability of the wind magnitude is high. Maximums of wind velocities were detected in 2002, 2005, 2006, 2008, 2010, 2012, and 2015 (Fig. 8b). The weakening of the wind in the recent period and the previous century was obtained earlier in a number of studies from *in-situ* measurements (Repetin and Belokopytov, 2008, 2009; Ilyin et al., 2012; Onea and Rusu, 2014), that was related in Repetin and Belokopytov (2008) to the decline of number of atmospheric cyclones passing from the Mediterranean Sea.

High-resolution scatterometry data gives a unique possibility to investigate seasonal wind variability using measurement-based data on the small spatial scales. This is especially important for the understanding of the seasonal changes of wind in coastal mountain regions, where errors of the atmospheric models rise and meteostations data are not available. Maximum basin-averaged wind velocity is observed in winter and it is approximately 7 m/s in the QuikScat data and 6.5 m/s in the ASCAT data (Fig. 8a). In winter winds are on average northerly and northeasterly over the entire basin, except for the southeastern part (Fig. 9a,b). In the southeastern basin the average winds are near zero, that means that winds here have various directions. Off the eastern coast the average winds have southeasterly direction. Such a feature of the eastern basin is, firstly, related to the blockage of general large-scale winds by the Caucasus Mountains. Due to the blockage, the pressure is

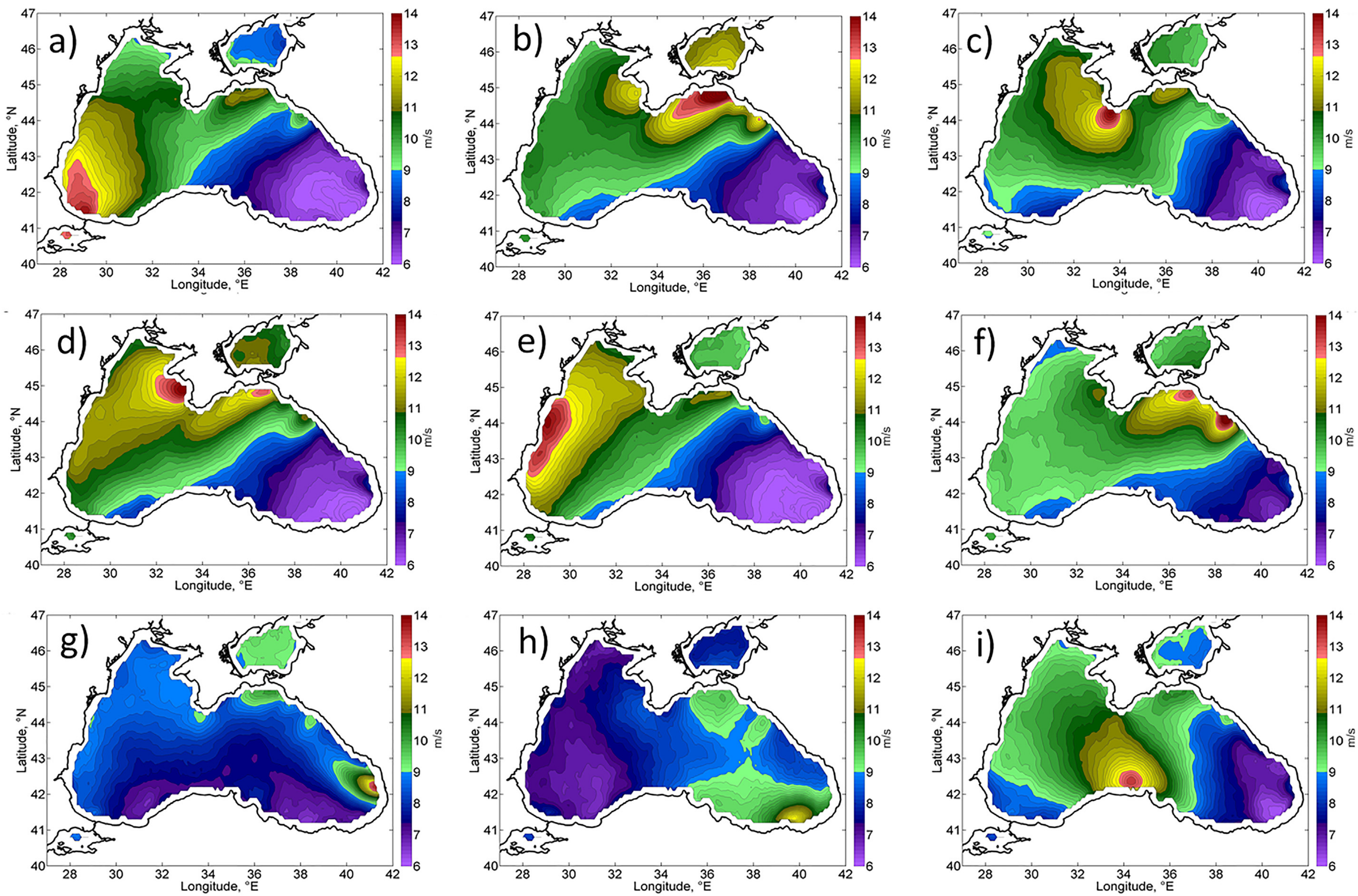

Fig. 7. Composite maps of wind magnitude (m/s) for wind velocity exceeding 95 percentile in the area of: a) H1 – near the Bosphorus (29.1°E, 41.5°N); b) H2 (36.8°E, 44.85°N) – the Kerch Strait; c) H3 (33.6°E, 44.25°N) – southwestern Crimea; d) H4 (33.2°E, 44.9°N) – western Crimea; e) H5 – the western Black Sea coast (29°E, 44.05°N); f) S2 – Tuapse (38.5°E, 44.1°N); g) S3 – the Kolkheti Lowland (41.2°E, 42.25°N); h) S4 – cape Fener (39.8°E, 41.4°N); i) S5 - the southern central coast (32.7°E, 42.2°N).

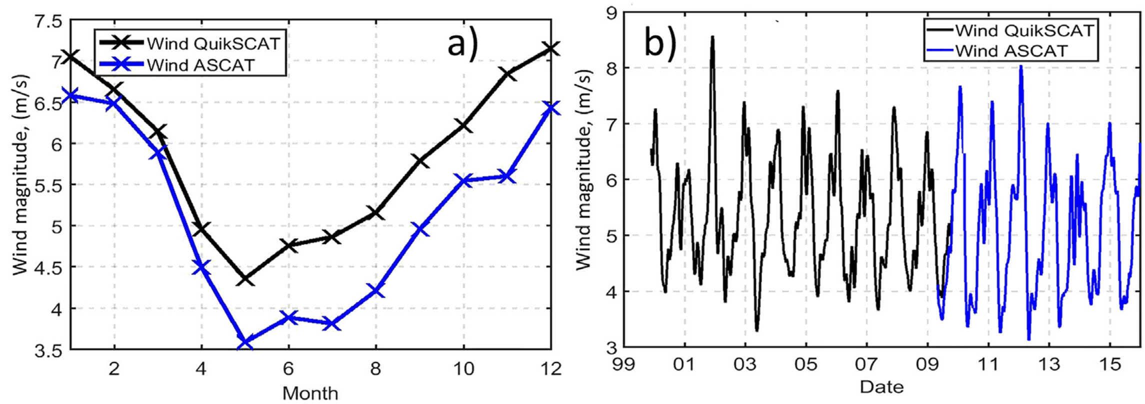

Fig. 8. a) Seasonal variability of wind magnitude (m/s) from the QuikScat in 2000–2009 (black line) and the ASCAT in 2011–2016 (blue line) data; b) interannual variability of wind magnitude (m/s) from the QuikScat (black line) and the ASCAT (blue line) data. To highlight relatively low-frequency wind variability on the seasonal time scales, the data were smoothed by a 30-day year moving average. (For interpretation of the references to color in this figure legend, the reader is referred to the web version of this article.)

lower over the eastern part of the basin and inflowing air rotates to the east forming an area with strong cyclonic vorticity. This effect is stronger during northerly winds, while during northeasterly winds they propagate almost without rotation to the southeast of the basin. The second important effect significantly modifying the wind velocity and curl characteristics is the Kolkheti valley winds (Pustovoitenko and Malinovsky, 1998; Alpers et al., 2011). Their effect is clearly observed on the seasonally-averaged wind velocity map (Fig. 9a,b). This effect is more prominent in the ASCAT data for 2010–2016 than in the QuikScat data for 2000–2009. Over the coastal areas in the west and north parts of the basin, the intensity of average winds is higher, which means that winds are more stable. The north direction of the winds in winter over the western coast is partly attributed to the local monsoon effect (Efimov and Anisimov, 2011b; Kubryakov et al., 2015), which also contributes to the cyclonic wind curl increase in this part of the basin.

The largest wind magnitudes in the winter period (7–9 m/s) are observed in the northwestern part of the sea (Fig. 10a,b). Minimum values are observed in the southeastern part (5–6 m/s) due to the winds being blocked by the Caucasus Mountains. The maximums of wind velocity (~9 m/s) are located along the major wind direction on the leeward side of the Kerch Strait and near the western and southern Crimea (maximums H2, H3, H4). These maximums are related to the discussed in Section 5 cape effect and gap (strait) effects. Also a small maximum is clearly seen near the Bosphorus (H1).

The wind rapidly decreases after winter and reaches its minimum in May (V = 3.5 m/s – in the ASCAT and V = 4.5 m/s in the QuikScat data) (Fig. 8a). In May the action of the Siberian and the Azores Anticyclones on the basin weakens and the impact of the large-scale atmospheric circulation on the Black Sea winds is minimal. Average winds in spring are near zero. Wind direction is very variable with the slight domination of northeasterly winds in the western part of the basin and westerly, northwesterly winds in the east part (Fig. 9c,d).

The winds intensity is relatively low from May to July (from 3.5 to 4.5 m/s in the ASCAT data and from 3.5 to 4.5 m/s in the QuikScat data). In these months, the local breeze or monsoon and orographic effects begin to play a more significant role in the Black Sea circulation. In April–July the sea is colder than the land in the Black Sea region. This land-sea temperature contrast drives the northward coastal winds in the western part of the basin (Efimov and Anisimov, 2011a,b; Kubryakov et al., 2015). The increase of the coastal winds in the western, southwestern and northeastern coastal areas is seen in the seasonally averaged QuikScat wind magnitudes map (green in Fig. 10c,e). Over the northwestern shelf, where the coast rotates these winds form a local anticyclonic circulation cell in May (Efimov and Anisimov, 2011a,b; Kubryakov et al., 2015). In the hot years these effects increase. They can noticeably impact the Black Sea circulation on the northwestern shelf and associated transport of nutrients, loaded in this part of the basin by large rivers (Kubryakov et al., 2018).

In summer the Black Sea is situated in the eastern periphery of the Azores Anticyclone and the northerly winds are generally observed. The Pontic Mountains blocks northerly winds, which results in the deviation of wind direction to the west in the western part and to the east in the eastern part (Fig. 9e,f). Average wind magnitudes in summer are the lowest (Fig. 10e,f). In the southeast they are on average approximately 3.5 m/s, in the northern part – up to 5 m/s. Average winds are highest in the western coastal part of the basin and over the Sea of Azov. According to the QuikScat data, their average magnitude here is ~6 m/s.

From August winds began to increase. In October–November the Siberian Anticyclone intensifies and it leads to the northeasterly winds over the basin (Fig. 9g,h). They are significantly higher in the northwestern part (6–7 m/s). Wind velocity is lower (4–5 m/s) in the southeast due to the topographic shadowing by the Caucasus Mountains. Several discussed previously maximums are well seen in the wind magnitude distribution: maximum near the Bosphorus, the Kerch Strait, southern Crimea, the western coast (Fig. 10g,h).

7. Spatial, seasonal and interannual variability of the wind curl

7.1. Average spatial variability

Fig. 11 shows a time-averaged wind curl map computed from the QuikScat and the ASCAT data. Both datasets show similar spatial distribution of wind curl. However the ASCAT wind curl is higher, especially in summer. This difference is partly related to the general rise of wind curl in 2003–2015 (see below). Secondly, the overestimation of low winds in the QuikScat dataset should decrease the wind gradients between the zone of strong winds and wind shadows (Section 3.2). These topographic effects play a very important role in the wind curl variability, which impacts the underestimation of the wind curl in the QuikScat data.

W is positive (cyclonic) in the eastern part of the sea with three very intense local maximums. On contrast, W over the west part of the sea is generally anticyclonic, in agreement with (Zecchetto and De Biasio, 2007; Efimov and Anisimov, 2011a), with maximum in the southwestern part of the sea ($1 * 10^{-5}$ 1/s). Different signs of wind curl in the eastern and the western parts of the Black Sea are related to several effects. Firstly, the blockage of northerly winds in the south turns the winds to the west (anticyclonically) in the western part and to the east (cyclonically) in the eastern part. This effect is observed both in warm and cold periods of a year. Secondly, winds flowing around the high Caucasus Mountains turn cyclonically and form a vast area of cyclonic vorticity in the eastern part of the basin. Thirdly, in the western part of

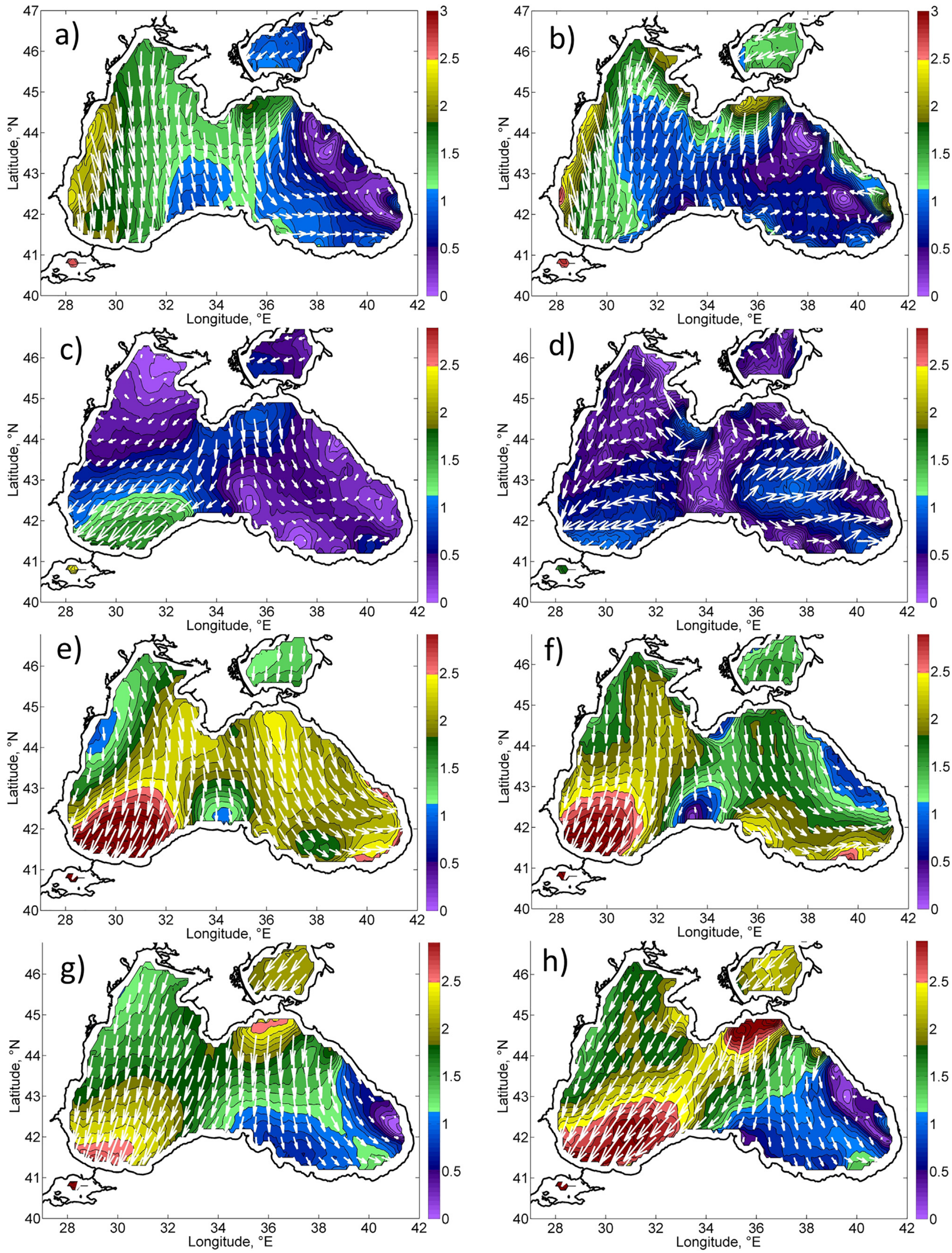

Fig. 9. Average wind maps (m/s) from the QuikScat (left) and the ASCAT (right) data for winter (December–February) (a,b), spring (March–May) (c,d), summer (June–August) (e,f), and autumn (September–November) (g,h). Scales of arrows are shown by color. (For interpretation of the references to color in this figure legend, the reader is referred to the web version of this article.)

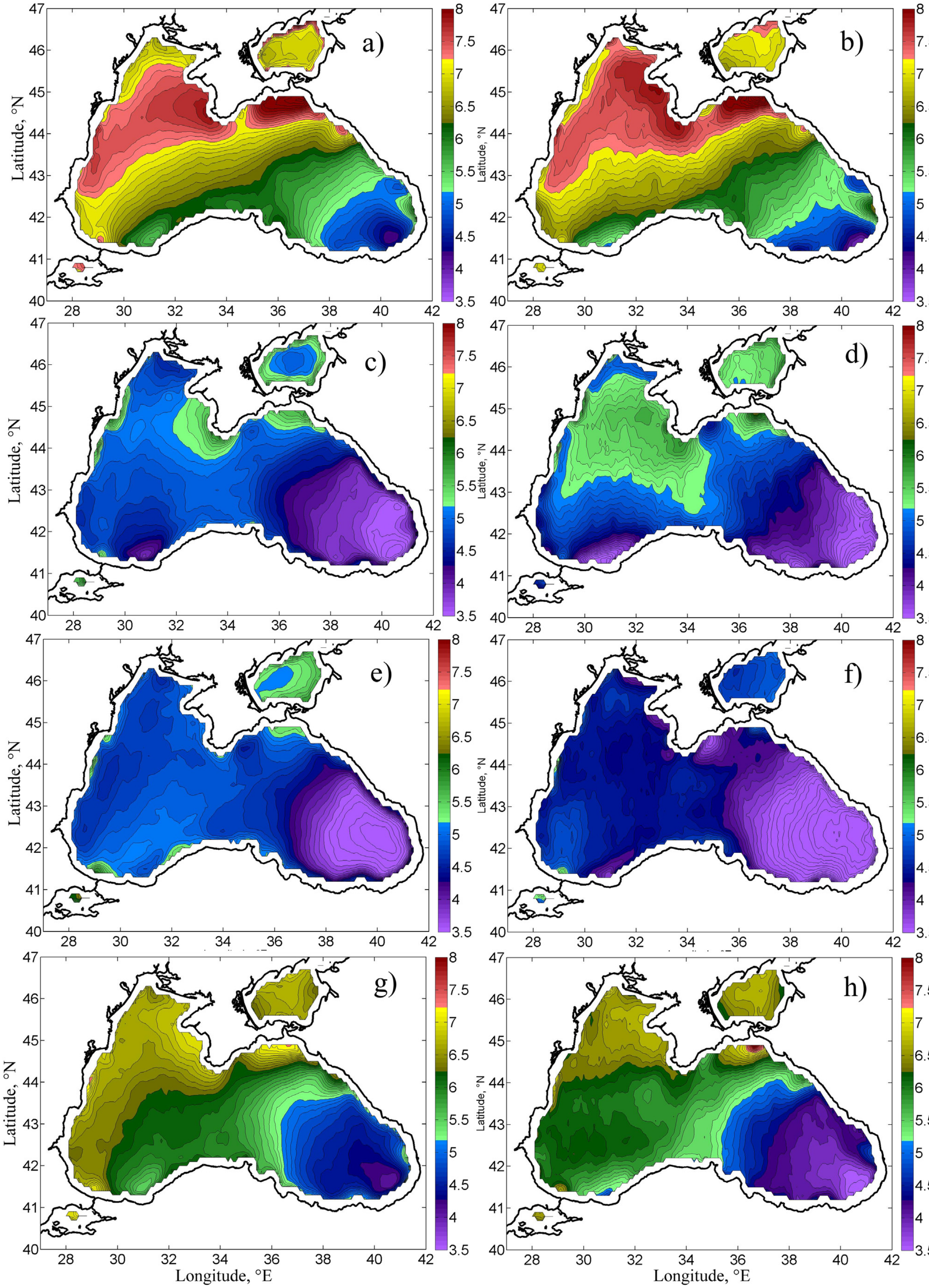

Fig. 10. Average wind magnitudes (m/s) from the QuikScat (left) and the ASCAT (right) data for winter (a,b), spring (c,d), summer (e,f), and autumn (g,h).

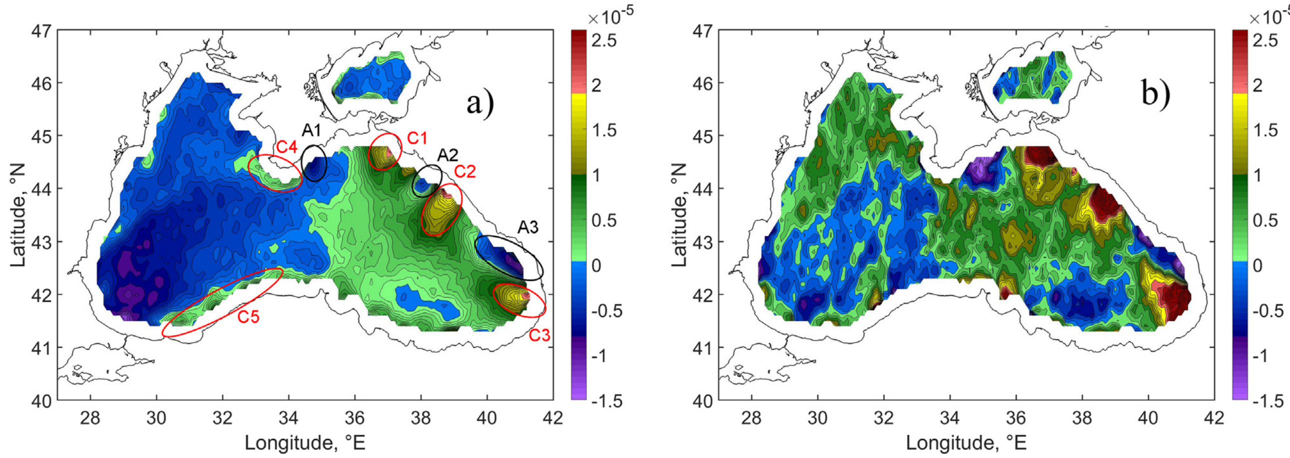

Fig. 11. Time-averaged wind curl distribution (1/s) from the measurements of QuikScat in 2000–2009 (a) and ASCAT in 2010–2016 (1/s).

the sea surrounded by the relatively flat terrain the monsoon effect forms a relatively strong anticyclonic circulation cell in summer (see also Efimov and Anisimov, 2011a).

Two local areas in the western part are cyclonic: area C4 to the west of Crimea; area C5 to the west of the central Pontic Mountains. Cyclonic wind curl in C4 is probably related to the cyclonic wind shear of the tip jets rounding the south of Crimea during northerly and northwesterly winds. This local increase of wind curl is observed mostly in summer. The cyclonic winds in area C5 are related to the flowing of air around the Pontic Mountains near the central Anatolian coast. Its position corresponds to the position of the observed wind shadow zone L1 related to the topographic blockage of the northeastern winds (Fig. 4d).

The local zone of anticyclonic vorticity A1 observed in the east Black Sea near the southeastern Crimea corresponds to the position of the zone of minimum velocity L2 (Fig. 4d). The blockage of northeasterly winds by Crimean Mountains leads to the anticyclonic wind shear on the western periphery of the winds blowing from the Kerch Strait.

Three maximums in the eastern side of the Black Sea give a very significant contribution to the overall cyclonic curl over the basin. Average W in these maximums is $> 2 * 10^{-5}$ 1/s. To understand the nature of these maximums, let us see in more detail the wind curl distribution in the eastern Black Sea in January (Fig. 12a,b). Strong northeasterly winds blow here through the Kerch Strait due to the action of large-scale circulation. Winds flowing through the Kerch Strait rotate into the low pressure area behind the Caucasus Mountains and form a large cyclonic vorticity cell in the box 43°–45°N 37°–39°E. Two northern maximums (C1 and C2) can be represented as one large divided in the center by the local area with anticyclonic vorticity. The position of this area corresponds to the position of the wind maximum S2 (Fig. 4f), related to the local lowering of the mountains near Tuapse (see Section 5). Wind jets flowing through this gap create anticyclonic wind shear A2 (centered in point 44°N, 38.2°E) in the right (northern) part of the gap and the zone of cyclonic wind shear C2 to the left (south) of the gap. The cyclonic shear on the left (southeastern side) of the strongest northerly and northwesterly winds blowing from the Kerch Strait results into the local maximum of wind curl C1.

The third maximum C3 in the southeastern part of the sea is related to the valley winds from the Kolkheti Lowland. The combination of average northerly winds in the eastern part of the sea and the opposite

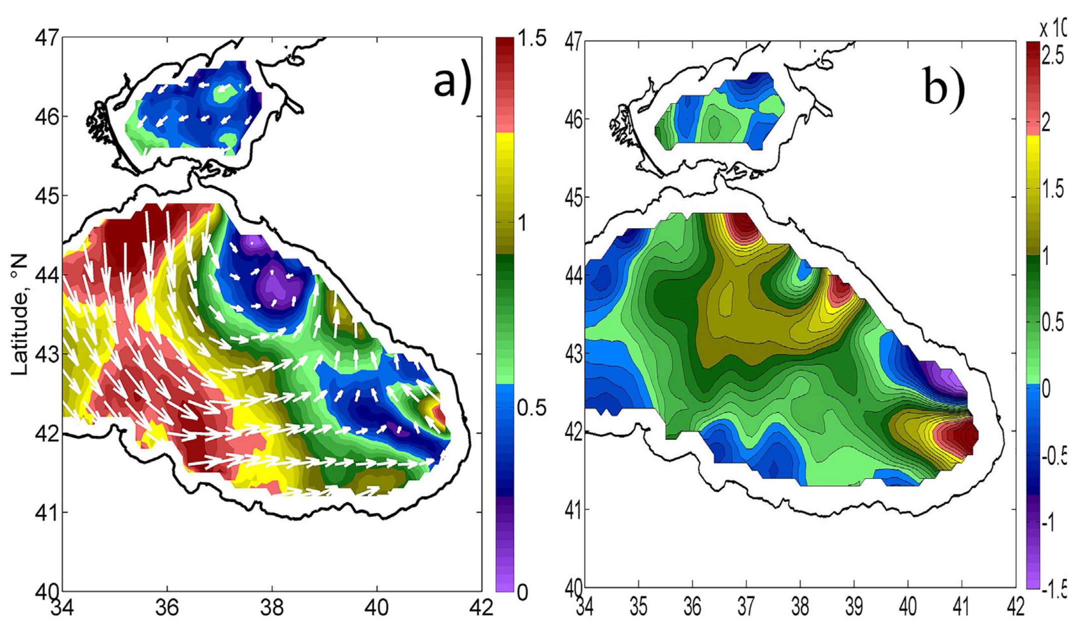

Fig. 12. Map of time-averaged wind (m/s) and wind curl (1/s) in January of 2000–2009 from the QuikScat data. Scales of arrows are shown by color. (For interpretation of the references to color in this figure legend, the reader is referred to the web version of this article.)

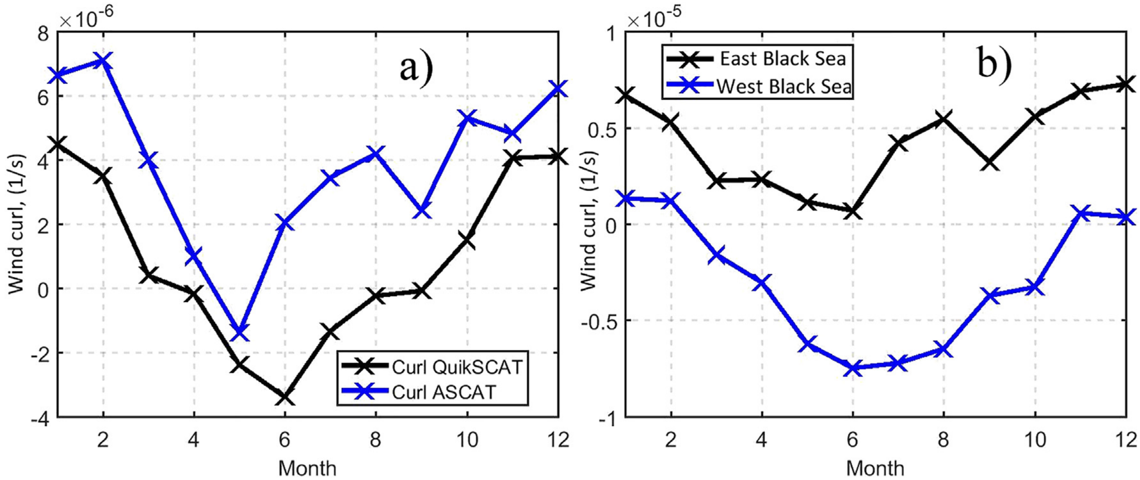

Fig. 13. Seasonal variability of a) basin-averaged wind curl (1/s) from the QuikScat (black line) and the ASCAT (blue line) data; b) basin-averaged wind curl (1/s) from the QuikScat in the western (27–35°E) (black line) and the eastern (blue line) (34–42°E) parts of the basin. (For interpretation of the references to color in this figure legend, the reader is referred to the web version of this article.)

southwesterly winds from the Kolkheti Lowland results into the generation of the third intense maximum of W on the left side of the Kolkheti jet. The jet rotates slightly to the right over the sea, resulting into the formation of the area A3 of the strong anticyclonic curl to the east of the jet.

The total contribution of discussed three local maximums to the cyclonic vorticity over the basin can be computed from the average wind curl distribution. For this task, we calculate the summary curl in the points, where curl is $> 10^{-5}$ 1/s, $W_{locmax} = \sum_i \overline{W_i}(\overline{W_i} > 10^{-5})$. Here $\overline{W}$ is time-averaged curl in a point. Such large values in the time-averaged maps corresponded only to the areas of maximums C1–C3. Then we divide W_{locmax} on the sum of all positive values of average wind curl $W_{cyclonic} = \sum_i \overline{W_i}(\overline{W_i} > 0)$. The computed contribution is equal to 30% according to Q data, and it reaches > 45% according to A data. The impact of three local maximums C1–C3 related to the small-scale topographic effects is of considerable importance for the wind curl over the Black Sea, and related basin dynamics.

7.2. Seasonal variability of wind curl

Seasonal variability of basin-averaged wind curl and its seasonal maps are given in Figs. 13, 14. On average the wind curl over the basin is cyclonic, with maximum in winter and minimum in May–June (Fig. 13a). Throughout the year the spatial structure of wind curl is similar to its average structure (Fig. 14). The curl is mostly anticyclonic in the west of the basin and cyclonic in the eastern Black Sea. The three discussed intense cyclonic maximums (C1–C3) in the eastern part are observed in all seasons of the year, except summer, where only one maximum C2 is observed. The three discussed minimums near the southeastern Crimea, to the north of the Kolkheti valley winds and to the north of Tuapse (A1,A2,A3), are also observed in all seasons. Generally, the values of W in the local maximums and in the eastern part are significantly higher in all seasons in the ASCAT dataset. This is probably related to the underestimation of wind gradients between wind jet and wind shadows zones in the QuikScat dataset (see Section 3.2).

The maximum basin-averaged W is observed in December–February with values of $5 * 10^{-6}$ 1/s in the QuikScat dataset and $7 * 10^{-6}$ 1/s in the ASCAT dataset, respectively (Fig. 13a).

Seasonal variability of the basin-averaged wind curl in the western (27–35°E) (black line) and eastern (blue line) (34–42°E) parts of the basin from the QuikScat data is shown in Fig. 13b. Average values of W in the western part are ($-2 * 10^{-6}$ 1/s), which is significantly lower than in the eastern part ($4 * 10^{-6}$ 1/s). At the same time, their seasonal variability is similar: maximum is observed in winter, minimum – in summer. The eastern part gives a major contribution to the total cyclonic curl in winter with values of $W = 7–8 * 10^{-6}$ 1/s, compared to only $W = 1–2 * 10^{-6}$ 1/s for the western part.

In the western part of the sea surrounded by the relatively flat terrain one of the major factors driving W seasonal variability is the monsoon effect. In winter the land-sea temperature contrasts reach maximal negative values (Korotaev et al., 2001; Efimov and Anisimov, 2012). The pressure difference results in the formation of alongshore cyclonic winds (Kubryakov et al., 2015) and the general cyclonic circulation of the basin. This effect, particularly, causes the cyclonic W over the northwestern part of the basin (Fig. 14a,b), where basin orography and, thereby, alongshore winds rotate. In the southwestern part, the curl in winter is still anticyclonic, which is related to the anticyclonic shear on the north periphery of the large-scale northeasterly winds.

In the eastern part of the basin the topographic effects, acting simultaneously with the monsoon effect, gives a major contribution to cyclonic W. The three discussed above local maximums and minimums of W intensify in winter. The orographic small-scale effects (valley and gapwinds, strait effects, cape effects, and topographic blocking) are the most intense during winter, as the winds and pressure differences between the sea and the land are the strongest. In winter additional maximum (C4) is seen in the southeastern part near the Kaliakra cape (36°E, 42°E). This maximum is probably associated with the sharp rotation of the northerly winds to the east in this point due to their blockage by the Pontic Mountains.

In May–July the land-sea temperature contrasts change sign and become positive, while anticyclonic alongshore winds are observed in the western part of the basin (Efimov and Anisimov, 2012; Kubryakov et al., 2015). In May–September, the Azores Anticyclone is affecting the Black Sea. It brings the northerly and northwesterly winds, inducing anticyclonic vorticity in the western part and cyclonic vorticity in the eastern part of the sea. Both large-scale circulation and monsoon effect decrease cyclonic curl over the basin. In spring the high values of cyclonic vorticity are observed only near the eastern coast of the basin, which is related to the impact of the discussed above topographic effects (Fig. 14e,f). Basin-averaged curl is minimal in May, which corresponds to the month of the most positive land-sea temperature contrasts (Kubryakov et al., 2015).

Basin-averaged W in the QuikScat data is anticyclonic during five months in a year (from May to September) with average values of $W = -2 * 10^{-6}$ 1/s (Fig. 13a). In the ASCAT data average wind curl is negative only in May, and in summer it is cyclonic (Fig. 13a). Generally,

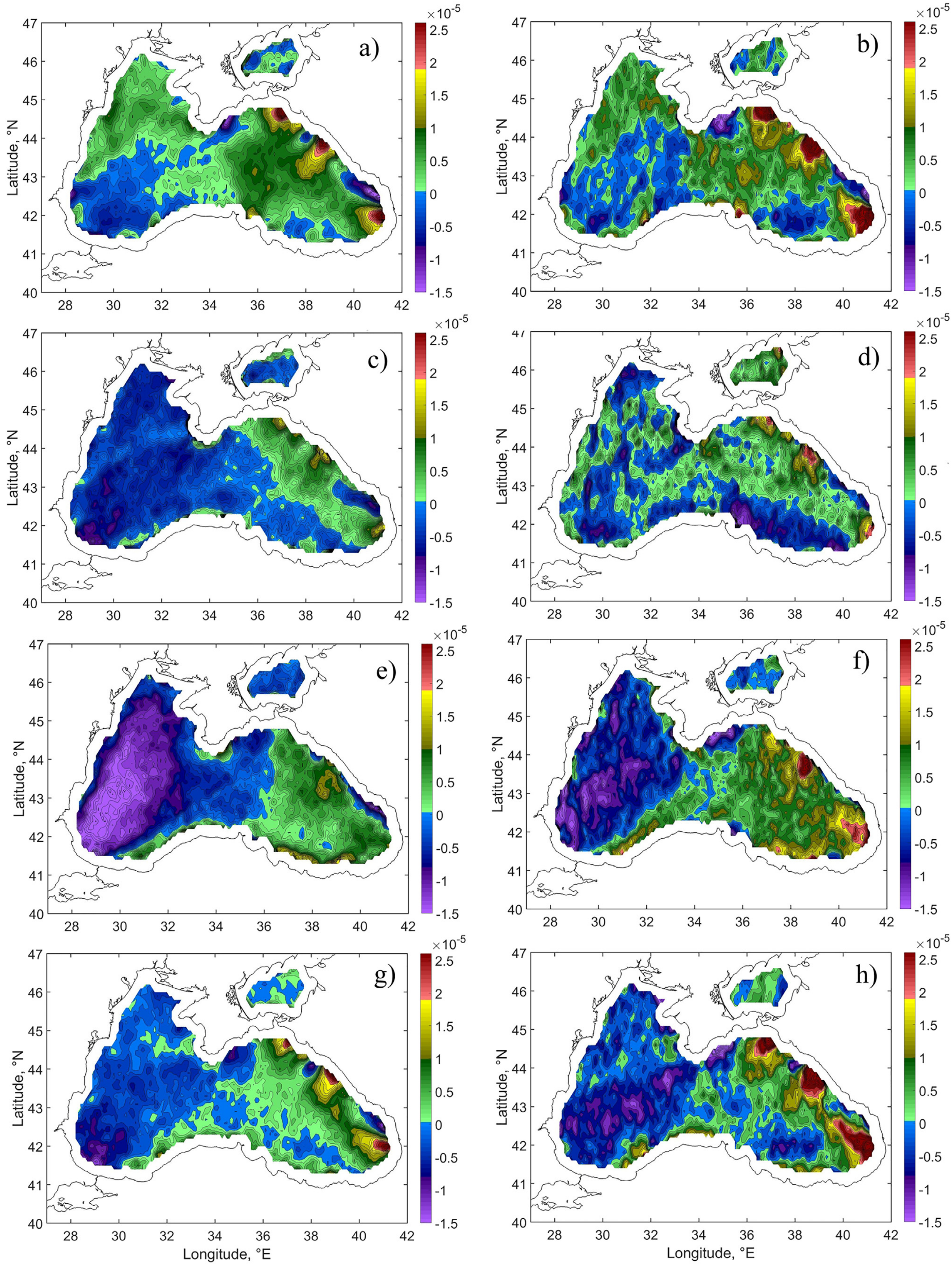

Fig. 14. Wind curl (1/s) from the QuikScat (left) and the ASCAT (right) data for winter (a,b), spring (c,d), summer (e,f), and autumn (g,h).

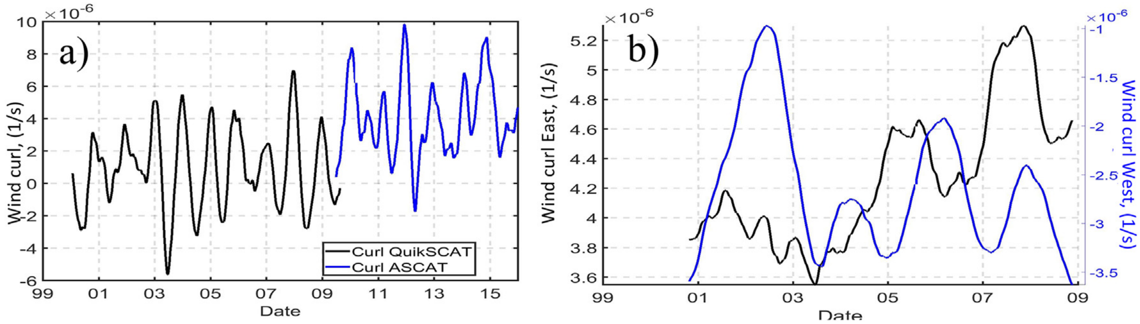

Fig. 15. The interannual variability of a) basin-averaged wind curl (1/s) from the QuikScat (black) and the ASCAT (blue) data (time series are smoothed by a 90-day moving average to demonstrate changes in the seasonal variability of the wind curl); b) average wind curl from the QuikScat (1/s) in the western (black) (27–35°E) and eastern (blue) (34–42°E) part of the basin (time series are smoothed by 1-year moving average to highlight wind changes on the annual time scales). (For interpretation of the references to color in this figure legend, the reader is referred to the web version of this article.)

in summer the anticyclonic circulation over the whole western part is very intense. It reaches average values of $W = -7 * 10^{-6}$ 1/s according to the QuikScat data, which is close to the winter values of cyclonic curl in the eastern part of the sea (Fig. 13b). W is cyclonic only off the southwestern coast and to the south of Crimea (Fig. 14e,f). This is related to cyclonic shear at the left side of the northeasterly winds, and tip jets around the Crimean Peninsula.

The topographic effects are significantly stronger in summer in the second period (2010–2015) according to the ASCAT data (Fig. 14). Particularly, in the QuikScat data for 2000–2009 in summer only one maximum (C2) is observed in the eastern part of the basin. This maximum is associated with the generation of the Caucasus coastal cyclone formed as a result of gap winds rotation near Tuapse (Efimov et al., 2009; Shokurov, 2011). At the same time in the ASCAT data another maximum, C3, related to the Kolkheti valley winds, is also observed.

The secondary peak of basin-averaged cyclonic curl is observed over the eastern Black Sea in August (Fig. 13b). It is probably related to the elongation of the Azores Anticyclone to the east, observed in August (not shown). Flowing of northerly winds on their eastern periphery around the Caucasus Mountains increases the intensity of topographic effects (such as the formation of the Caucasus Anticyclone (Shokurov, 2012; Efimov and Barabanov, 2013)), and cyclonic curl in the eastern part of the sea.

September is the intermediate month between the change of

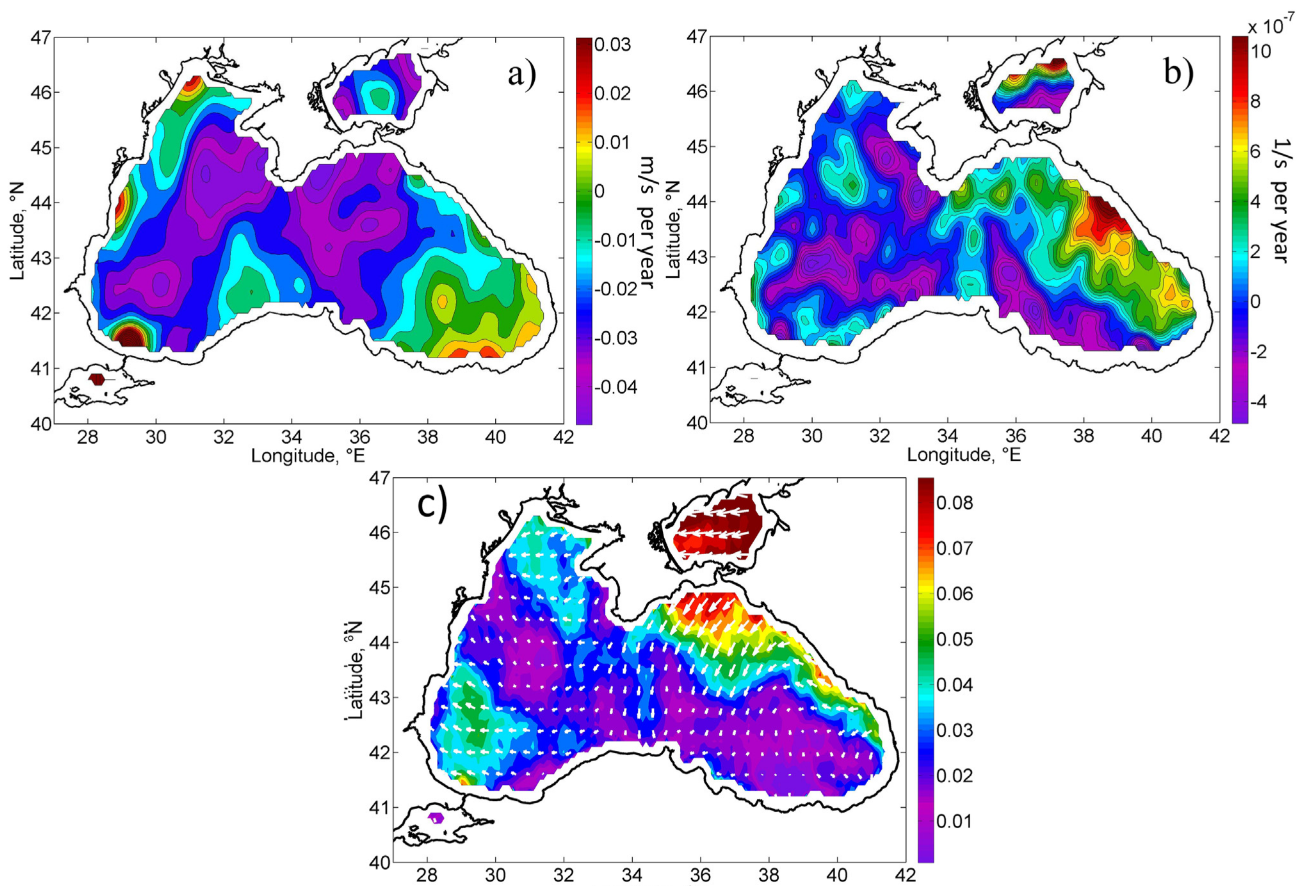

Fig. 16. Spatial trends of wind velocity (m/s per year) (a), wind curl (1/s per year) (b) and wind components (m/s per year) (c) from the QuikScat data in 2000–2009. Scales of arrows are shown by color. (For interpretation of the references to color in this figure legend, the reader is referred to the web version of this article.)

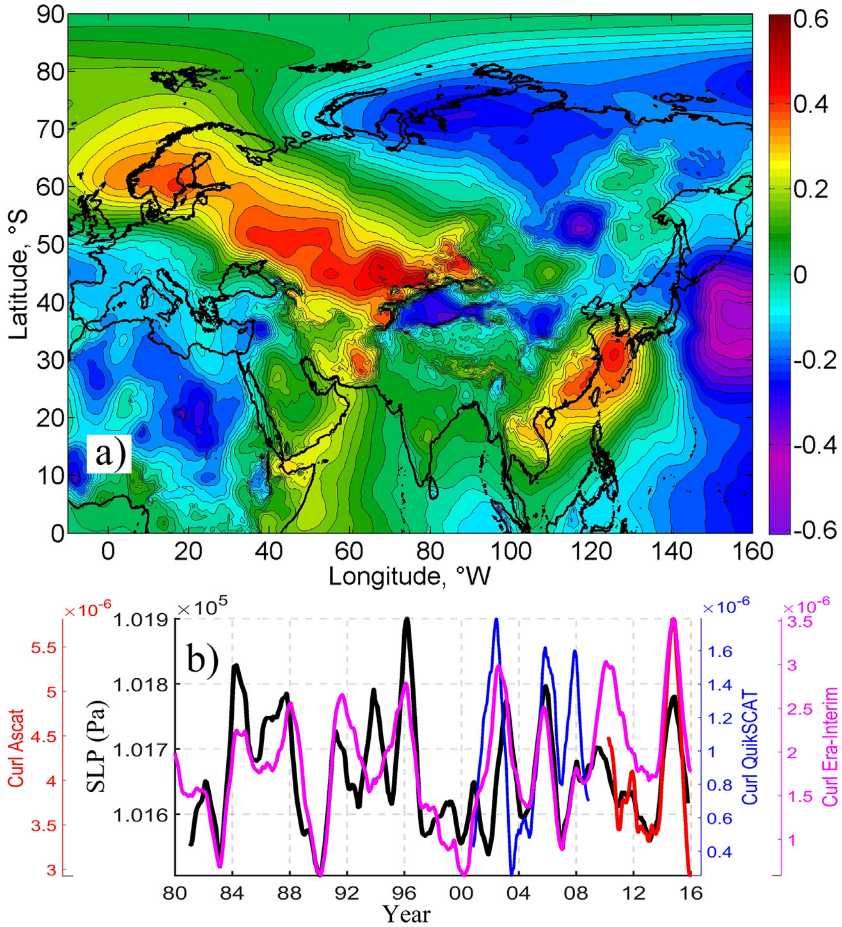

Fig. 17. a) The correlation map between the basin-averaged wind curl and the SLP variability in every grid point from the Era-Interim reanalysis data for 1979–2016; b) interannual variability of the SLP (Pa) near Belgorod, Russia (50.5°N, 36.5°E) (black line) and wind curl (1/s) from the Era-Interim (purple), the QuikScat (blue) and the ASCAT (red). Time series are smoothed by a 1-year moving average to highlight wind changes on the annual time scales. Note different color scale limits. (For interpretation of the references to color in this figure legend, the reader is referred to the web version of this article.)

dominance of the Azores and the Siberian Anticyclones. That is why in September northerly winds in the eastern Black Sea decline and W slightly decreases (Fig. 13a,b). In October the action of the Siberian Anticyclone increases over the basin. This induces the rise of the northeasterly winds and sharp increase of cyclonic vorticity in the eastern part of the sea, related to a number of topographic effects. Rapid cooling of land surface temperature in comparison to sea temperature increases monsoon cyclonic winds in the basin. The distribution of W in autumn resembles the winter distribution.

7.3. Interannual variability of wind curl

The interannual variability of the wind curl (Fig. 15a) shows that the largest minimum of wind curl was observed in summer of 2003. After 2003 the wind curl rises. Strong maximums are observed further in winters of 2004, 2008, 2010, 2012, and 2015. The same rise of wind curl was detected in the Era-Interim reanalysis during 1979–2015 (Kubryakov et al., 2017).

Interestingly, the interannual variability of the wind curl in the

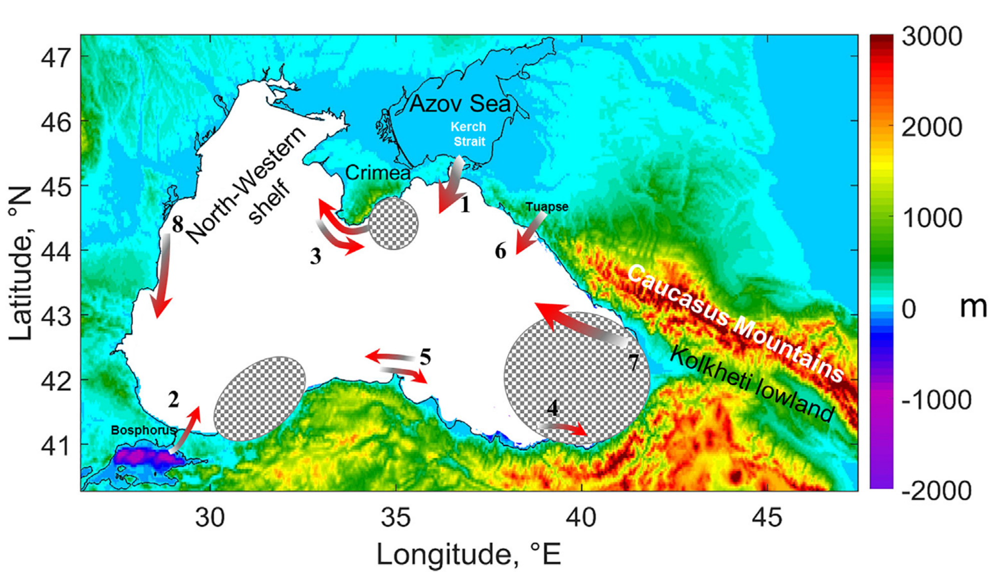

Fig. 18. A scheme summarizing small-scale wind effects discussed in the study: shaded circles – zones of wind shadow; 1 – winds from the Kerch Strait; 2 – winds from the Bosphorus; 3 - tip jets near southern Crimea; 4 - tip jets near the cape Fener; 5 - tip jets near the capes on the central Anatolian coast; 6 – wind jets near Tuapse, Novorossiyskaya bora; 7 – the Kolkheti valley winds; 8 – winds along the western coast of the Black Sea.

western and eastern parts differs significantly (Fig. 15b). W in the western part of the sea was maximum in 2002–2003 ($W = -0.5*10^{-6}$ 1/s for the yearly-smoothed value) and then decreased to an average value of ($W = -3*10^{-6}$ 1/s). The biannual signal is well-seen in W variability in the west Black Sea: wind curl was maximum in the 2002, 2004, 2006, and 2008. On contrast, in the eastern part W constantly increases and near-4-5-year oscillations can be observed. The minimal values were observed in 2000–2003 ($\sim 3.5*10^{-6}$ 1/s) and maximal - in 2008 ($\sim 5*10^{-6}$ 1/s), with the secondary peak in 2005–2006 ($\sim 4.5*10^{-6}$ 1/s). Such differences are related to the completely different mechanism driving wind curl variability in the western and eastern Black Sea – the impact of topographic effects in the eastern part and large-scale atmospheric effects in the western part (see Section 7).

The rise of the cyclonic wind curl, caused by its variations in the eastern part, is observed simultaneously with the general decrease of wind velocity over the basin. The possible reasons of these changes are briefly discussed further.

8. Discussion

8.1. Impact of large-scale atmospheric circulation on long-term wind changes

The long-term changes of the Black Sea wind characteristics – decrease in wind velocity (Repetin and Belokopytov, 2008, 2009; Ilyin et al., 2012) and increase in wind curl (Kubryakov et al., 2017) are tightly related to the changes of the large-scale atmospheric circulation.

The map in Fig. 16a shows the spatial distribution of wind magnitude trends from the QuikScat data. Winds decrease significantly in the northeastern and western central parts of the sea with the value of trend $-\sim 0.05$ m/s per year. These places correspond well to the areas of the most intense northeasterly winds blowing in the cold period of a year (see Fig. 10). Thereby, dominant northeasterly winds, which are related to the action of the Siberian Anticyclone, decline later. On contrast, in the wind shadow zone in the southeastern part of the basin wind velocity slightly increases (0.01–0.02 m/s per year). Also, the trends are positive in coastal areas along the western coast, and in the vicinity of the Bosphorus. Coastal winds over the western coast are largely related to the local monsoon effect, which seems to intensify or keeps its intensity constant. Wind curl spatial trends (Fig. 16b) show that the largest changes are observed in the eastern part, where W rises significantly. Maximum W rise is observed near Tuapse (C2). Here W is increasing by $1*10^{-6}$ 1/s or $\sim$10% per year.

In the southeastern part of the basin the signs of trends of wind and wind curl coincide. Intensification of winds in this area is the probable reason of wind curl increase. To understand the long-term changes of the wind direction over the basin, the linear trends (kx,ky) of the wind components u,v were calculated in every grid point (Fedorov et al., 2017). Then the vectors kx,ky representing the tendency of directional wind change were plotted (Fig. 16c). We can see that the most changes occur in the eastern part of the Black Sea and over the Sea of Azov. Over the Sea of Azov the eastward direction becomes more dominant and average wind direction changes from north-north-east to north-east-east. The northeasterly winds generally increase over the northeastern part of the basin near the Kerch Strait. At the same time in the western part we observe only a small increase in the westward wind component.

In the coastal eastern part of the basin we observe a noticeable increase of northwesterly winds. These winds are largely related to the topographic blockage of the north winds, which further turns cyclonically around the eastern Black Sea and form a vast area of intense cyclonic vorticity in the eastern Black Sea. This is different to the more typical situations when northeasterly winds are blowing from the Kerch Strait to the Marmara Sea. In these cases winds are only partially blocked in the southwest by the western Pontic Mountains. In such situations maximum winds are observed in the southwest Black Sea and the generated cyclonic vorticity is associated only with the wind shear on their southern flank. Thereby, relatively small changes in the wind direction from southward to southeastward completely changed the wind curl distribution over the basin. The increase of the Kolkheti valley winds may also contribute to the observed intensification of southeastern winds in this area. Southeastern winds in the eastern Black Sea significantly increase the wind curl there.

Winter winds over the Eurasia and the Black Sea strongly depend on the strength and position of the Siberian Anticyclone (*e.g.* Panagiotopoulos et al., 2005; Krivosheya et al., 2012). We use the Era-Interim reanalysis data for 1979–2016 to understand the relation between the sea level pressure (SLP) distribution in Eurasia and the wind curl over the Black Sea. The correlation map between basin-averaged W and SLP in every grid point is presented in Fig. 17a. Before the calculations, the data were smoothed by a 1-year moving average. The highest correlation ($k \cong 0.6, 0.7$) is observed over the southwestern Asia and eastern Europe. At the same time negative correlation is observed over the northeastern Asia. The increase of SLP over the western Russia and the decrease over the eastern Eurasia may be induced by the shift of the Siberian Anticyclone to the southwest from its typical position. As a result, winds bring more cold continental air to the west in the European part of Russia, situated to the north of the Black Sea. Cold air increases north-south gradients of temperature and pressure between the cold land and the warm Black sea. The higher pressure difference is the probable reason of stronger north wind flow around the Caucasus Mountains. The intensification of the north winds over the basin increases the wind curl over the eastern part of the Black Sea as was discussed above.

Sea level pressure to the north of the eastern Black Sea can be regarded as a precursor of wind curl change over the basin. As an example we take the SLP from the Era-Interim reanalysis near Belgorod, Russia (50.5°N, 36.5°E). The graph of interannual variability of the pressure in this point (black line) and the wind curl from the Era-Interim (purple line), the QuikScat (blue line) and the ASCAT (red line) data is presented in Fig. 17b. On interannual time scales the SLP at (50.5°N, 36.5°E) correlates with the Era-Interim wind curl with the coefficient of correlation 0.72. The correlation is also high for the QuikScat and the ASCAT data. It is clearly seen that almost all peaks of the wind curl are related to the change of pressure over eastern Europe. Maximums in 1984, 1988, 1991, 1996, 2002, 2006, and 2015 and minimums in 1983, 1990, 2000, and 2007 all are associated with the increase in pressure in the European part of Russia. Only two wind curl peaks in 1995 and 2008 are not described by the pressure variability. This result demonstrates that the position and strength of the Siberian Anticyclone is one of the main factors controlling interannual changes of the wind curl, and, thereby, the current intensity in the Black Sea.

8.2. Wind impact on the Black Sea dynamics

We can expect to observe the strongest effects of wind on the vertical mixing, mesoscale and submesoscale eddy dynamics, generation of internal waves and other important processes in the sea in the discussed above "hot-spots" of the Black Sea wind variability. These small-scale effects are summarized in Fig. 18.

Tip jets, gap winds and valley winds cause the sharp increase in local mixing and turbulence generation. The well-known example is the effect of the tip jets of southern Greenland, cape Farewell (Moore and Renfrew, 2005). These winds induce strong tip-jet-forced convection, which plays a significant role in the formation of the Labrador Sea water, an important part of the ocean conveyor (Pickart et al., 2003).

Similar increase in winter convection and, particularly, the Cold Intermediate Layer (CIL) formation due to the buoyancy loss should occur in the mentioned above maximums of wind in the Black Sea. Thereby, the areas near the Kerch Strait, the Bosphorus, southern Crimea, Tuapse, the Kolkheti valley, the capes on the Anatolian coast can be represented as "hot-spots" of the vertical mixing. Especially intense mixing and vertical entrainment of the deep waters is expected to occur in the local maximums in the eastern part of the basin. Here mechanical wind mixing is accompanied by strong upwelling, induced by the cyclonic curl intensification and the Ekman pumping. These zones can also be regarded as a significant source of oxygen which ventilates the Black Sea deep layers due to winter convection. The entrainment of the rich in nutrients deep waters in the upper euphotic layer may be the reason of the increase in the biological productivity in the zones of wind and wind curl maximums, and the observed spatial heterogeneity of biological species (Zatsepin et al., 2007; Kubryakov et al., 2019).

Horizontal shear of the surface currents caused by coastal jets induces the formation of the mesoscale ocean eddies of different signs (Fedorov and Ginsburg, 1989; Zatsepin et al., 2003, 2019; Zamudio et al., 2006): anticyclones on the right side and cyclones on the left side of the jet. Definitely, the enhanced mesoscale activity is often observed in the Black Sea in the discussed areas of strong wind coastal jets: Caucasus eddies are formed in the central eastern part of the basin, Batumi eddies – in the southeast, Kerch eddies – in the vicinity of the Kerch Strait, Sevastopol eddy – to the west of Crimea (Oguz et al., 1993; Korotaev et al., 2001; Ginzburg et al., 2002). Although other processes are important for the eddy formation (*e.g.* baroclinic instability of the Rim Current (Zatsepin et al., 2005; Kubryakov and Stanichny, 2015a)), wind shear and the Ekman pumping can contribute to their formation. Different sign of shear near the wind jets induces downwelling to the right of the jet and upwelling to the left of the jet. This can contribute to the oscillations of pycnocline and create initial disturbances that generate internal or shelf waves. They may create initial disturbances of the flow, that will later grow due to the baroclinic instability and form mesoscale eddies. For example, direct Ekman pumping is shown to be the reason of the anticyclones formation in the northwestern shelf (Korotaev et al., 2001; Grégoire and Lacroix, 2003; Kubryakov et al., 2017) and off the Caucasian coast (Zatsepin et al., 2003), and mesoscale cyclone formation in the southeast part of the basin (Kubryakov and Stanichny, 2015b).

Coastal wind jets induce cross-isobaths wind-driven currents that can effectively transport rich in nutrients and pollutants shelf waters to the deep basin (Ilyin et al., 1999; Zhou et al., 2014; Kubryakov et al., 2017). These processes are important for the ventilation of the shelf areas and biological productivity in the deep Black Sea. Strong wind pulses may be a reason of the generation of submesoscale eddies in the coastal zone, which impact the transport and accumulation of suspended matter in these areas (Zatsepin et al., 2019). Particularly, northerly winds over the western Crimean coast lead to the formation of strong current jets and a number of submesoscale eddies (Aleskerova et al., 2015). They effectively transfer the suspended matter released in the waters during storms in the basin center, impacting the cross-shelf exchange. Local places of wind maximums are the source of powerful surface waves. Storm winds and waves are dangerous for the coastal economy and maritime safety.

Wind curl is the main force driving the Black Sea circulation. The main feature of the basin circulation is the large-scale cyclonic Rim Current encircling the basin over continental slope. The Rim Current variability on the interannual and seasonal time scales correlates strongly with the basin-averaged wind curl (Stanev, 1990; Korotaev et al., 2001; Zatsepin et al., 2002; Kubryakov et al., 2016). However, even in summer, when the wind curl is on average anticyclonic (Fig. 13), the Rim Current is still directed cyclonically. This can be related to the current inertia and slow current deceleration (dissipation) after sharp increase in winter. On the other hand, anticyclonic eddies intensify in summer (Ivanov and Belokopytov, 2013; Kubryakov and Stanichny, 2015a). Probably, anticyclonic wind curl is one of the reasons of their intensification. Moreover, high anticyclonic curl in summer is observed in the western part of the sea, while wind curl is still positive in the eastern part. Therefore the forcing of the Rim Current is highly asymmetric: the western part of the sea decelerates the Rim Current, while the eastern part accelerates it again. How the current reacts on these changes and what happens in the intermediate zone between the western and the eastern parts is an open question.

Another interesting feature of the wind curl is the significant importance of the local small-scale maximums (up to 50%) on the total cyclonic curl. The Ekman pumping and the related Ekman divergence should somehow redistribute from these parts of the basin to increase average baroclinic energy of the Rim Current. The heterogeneity of wind curl forcing may result into different dynamical processes which are still poorly investigated at the moment,

9. Conclusions

Scatterometry measurements of the ASCAT and the QuikScat for > 15 years are used to investigate wind characteristics in the Black Sea. Comparison with *in-situ* measurements on the offshore platform shows that the QuikScat data overestimate wind velocity during low wind conditions ($V < 3$ m/s) by 0.5–1.5 m/s and underestimate strong winds ($V > 12$ m/s) in agreement with (Bentamy et al., 2008, 2012). The QuikScat dataset has more moderate winds ($V = 3$–11 m/s), while the ASCAT dataset has more peak minimal and maximal values. Particularly, the quantity of wind velocity with values < 2 m/s is 6% in the ASCAT and only 1% in the QuikScat array. Wind gradients between zones of strong wind jets and wind shadows play an important role for the generation of the cyclonic vorticity in the Black Sea. Overestimation of winds in wind shadows zones results in the underestimation of wind curl in the QuikScat data compared to the ASCAT dataset.

High resolution (12.5 km) satellite data gives a possibility to investigate small-scale features of the wind variability in the basin, mainly related to the topographic effects. This includes several wind shadow zones (near eastern Crimea, the southeastern Black Sea coast) and local maximums of wind velocity, which are related to the gap winds in the mountains and straits, valley winds from the Kolkheti Lowland and tip jets near the capes (near southern Crimea, several capes of the Anatolian coast). The small-scale wind features strongly impact the curl generation in the basin. Wind flow around the topographic obstacles is one of the major reasons of the cyclonic curl generation in the basin. Three small-scale wind curl maximums in the eastern part of the basin, related to the gap winds in the Kerch Strait and near Tuapse, and the Kolkheti valley winds with the size of ~50 km, contribute up to 45% to the total cyclonic curl over the basin according to the ASCAT data and ~30% - according to the QuikScat data.

We provide an analysis of seasonal and interannual variability of the wind velocity and curl from scatterometry measurements. The large-scale wind field is determined by the interplay between the dominance of the Siberian Anticyclone in winter and the Azores Anticyclone in summer. Seasonal changes of monsoon winds related to land-sea temperature differences impact local winds near the coast, especially in the western part of the basin and the northwestern shelf with flat relief. Small-scale topographic effects modulated by seasonal large-scale winds variability play an important role in all seasons of a year. During summer, wind curl is anticyclonic in the western part of the basin, where it is related to the impact of the Azores Anticyclone and anticyclonic monsoon winds. It is cyclonic in all seasons in the eastern part of the sea, which is mainly related to the topographic effects. The data on seasonal variability of wind velocity and curl are in agreement and complement the previous investigations (Sorokina, 1974; Efimov et al., 2002; Zechetto et al., 2007; Efimov and Anisimov, 2011a, 2012; Efimov and Barabanov, 2013; Kubryakov et al., 2015).

On interannual time scales the wind velocity in 2000–2015 decreases in agreement with the trend in the 20th century (Repetin and Belokopytov, 2008; Ilyin et al., 2012). At the same time the wind curl increases. The interannual variability of the wind curl in the eastern and the western parts of the Black Sea is completely different, which is related to the different driving mechanisms. The rise of wind curl is observed only in the eastern coastal part of the basin. We suggest that these trends may be associated with the change of wind direction from northeasterly to northerly over the eastern Black Sea. Northerly winds blocked by the Pontic Mountains in the south and the Caucasus Mountains in the east rotate cyclonically in the eastern Black Sea, which strongly increases the wind curl. These changes in wind characteristics can be related to the displacement of the Siberian Anticyclone to the west and result in the rise of north-south gradients of temperature and pressure between the continent and the Black Sea. The increase in the pressure differences intensifies northerly winds and wind curl over the eastern Black Sea. The sea level pressure over western Russia correlates strongly with the wind curl over the basin and may be regarded as a proxy for the changes in the Black Sea atmospheric and sea dynamics.

The discussed small-scale features of the wind field over the Black Sea can significantly impact the Black Sea mesoscale and large-scale dynamics. A detailed study of the physical processes driving small-scale maximums of wind variability is a subject of our next investigations.

Acknowledgments

The validation and intercomparison of scatterometry data was made under FASO contract no. 0827-2019-0002. The validation and intercomparison of scatterometry data was supported by RFBR, Russia, grant 19-05-00752a. Study of the small-scale wind variability was supported by RFBR, Russia, grant 19-05-00479a. Seasonal and interannual wind curl variability is investigated with support of RFBR, Russia, grant 17-05-41102RGO_a

References

Accadia, C., Zecchetto, S., Lavagnini, A., Speranza, A., 2007. Comparison of 10-m wind forecasts from a regional area model and QuikSCAT scatterometer wind observations over the Mediterranean Sea. Mon. Weather Rev. 135 (5), 1945–1960.
Akpinar, A., de León, S.P., 2016. An assessment of the wind re-analyses in the modelling of an extreme sea state in the Black Sea. Dyn. Atmos. Oceans 73, 61–75.
Aleskerova, A.A., Kubryakov, A.A., Stanichniy, S.V., 2015. Rasprostranenie vzveshennogo veshchestva pod vliyaniem shtormovykh vetrov u zapadnogo poberezh'ya Kryma po opticheskim dannym vysokogo razresheni [Suspension distribution under the influence of the storm winds near the western coast of the Crimea according to the high resolution optical data]. Sovr. Probl. DZZ Kosm. 12 (1), 63–71 (in Russian).
Aleskerova, A.A., Kubryakov, A.A., Goryachkin, Yu.N., Stanichny, S.V., 2017. Propagation of waters from the Kerch Strait in the Black Sea. Phys. Oceanogr. 6.
Alpers, W., Ivanov, A., Horstmann, J., 2009. Observations of bora events over the Adriatic Sea and Black Sea by spaceborne synthetic aperture radar. Mon. Weather Rev. 137 (3), 1150–1161.
Alpers, W., Ivanov, A.Y., Dagestad, K.F., 2011. Encounter of foehn wind with an atmospheric eddy over the Black Sea as observed by the synthetic aperture radar onboard Envisat. Mon. Weather Rev. 139 (12), 3992–4000.
Arkhipkin, V.S., Gippius, F.N., Koltermann, K.P., Surkova, G.V., 2014. Wind waves in the Black Sea: results of a hindcast study. Nat. Hazards Earth Syst. Sci. 14 (11), 2883.
Belokopytov, V.N., Fomin, V.V., Ingerov, A.V., 2017. On Multidisciplinary Investigations of Dangerous Natural Phenomena in the Azov–Black Sea Basin.
Bentamy, A., Croize-Fillon, D., Perigaud, C., 2008. Characterization of ASCAT measurements based on buoy and QuikSCAT wind vector observations. Ocean Sci. 4 (4), 265–274.
Bentamy, A., Grodsky, S.A., Carton, J.A., Croizé-Fillon, D., Chapron, B., 2012. Matching ASCAT and QuikSCAT winds. J. Geophys. Res. Oceans 117 (C2).
Burman, E.A., 1969. Local Winds (in Russian). Gidrometeoizdat (342 pp.).
Chelton, D.B., Schlax, M.G., Freilich, M.H., Milliff, R.F., 2004. Satellite measurements reveal persistent small-scale features in ocean winds. Science 303 (5660), 978–983.
Chronis, T., Papadopoulos, V., Nikolopoulos, E.I., 2011. QuickSCAT observations of extreme wind events over the Mediterranean and Black Seas during 2000–2008. Int. J. Climatol. 31 (14), 2068–2077.
Dee, D.P., Uppala, S.M., Simmons, A.J., Berrisford, P., Poli, P., Kobayashi, S., ... Bechtold, P., 2011. The ERA-interim reanalysis: configuration and performance of the data assimilation system. Q. J. R. Meteorol. Soc. 137 (656), 553–597.
Desbiolles, F., Bentamy, A., Blanke, B., Roy, C., Mestas-Nuñez, A.M., Grodsky, S.A., ... Maes, C., 2017. Two decades [1992–2012] of surface wind analyses based on satellite scatterometer observations. J. Mar. Syst. 168, 38–56.
Divinsky, B.V., Kos'yan, R.D., 2015. Observed wave climate trends in the offshore Black Sea from 1990 to 2014. Oceanology 55 (6), 837–843.
Ebuchi, N., Graber, H.C., Caruso, M.J., 2002. Evaluation of wind vectors observed by QuikSCAT/SeaWinds using ocean buoy data. J. Atmos. Ocean. Technol. 19 (12), 2049–2062.
Efimov, V.V., Anisimov, A.E., 2011a. Climatic parameters of wind-field variability in the Black Sea region: numerical reanalysis of regional atmospheric circulation. Izv. Atmos. Oceanic Phys. 47 (3), 350–361.
Efimov, V.V., Anisimov, A.E., 2011b. Numerical modeling of the influence of land–sea temperature contrasts on the atmospheric circulation in the Black-Sea region. Phys. Oceanogr. 21 (4), 221–229.
Efimov, V.V., Anisimov, A.E., 2012. Influence of the Black Sea on the regional climate. Morsk. Gidrofiz. Zh. (2), 37–49.
Efimov, V.V., Barabanov, V.S., 2013. Simulation of bora in Novorossiysk. Russ. Meteorol. Hydrol. 38 (3), 171–176.
Efimov, V.V., Komarovskaya, O.I., 2015. Spatial-temporal structure of bora in Yalta. Phys. Oceanogr.(3).
Efimov, V.V., Mikhaylova, N.V., 2017. The mesoscale atmospheric vortex as a manifestation of the Novorossiysk bora. Izv. Atmos. Oceanic Phys. 53 (4), 449–458.
Efimov, V.V., Yurovsky, A.V., 2017. Formation of vorticity of the wind speed field in the atmosphere over the Black Sea. Phys. Oceanogr. 6.
Efimov, V.V., Shokurov, M.V., Barabanov, V.S., 2002. Physical mechanisms of wind circulation forcing over the inland seas. Izv. Russ. Acad. Sci. Atmos. Oceanic Phys. 38 (2), 217–227.
Efimov, V.V., Shokurov, M.V., Yarovaya, D.A., 2007. Numerical simulation of a quasi-tropical cyclone over the Black Sea. Izv. Atmos. Oceanic Phys. 43 (6), 667–686.
Efimov, V.V., Stanichnyi, S.V., Shokurov, M.V., Yarovaya, D.A., 2008. Observations of a quasi-tropical cyclone over the Black Sea. Russ. Meteorol. Hydrol. 33 (4), 233–239.
Efimov, V.V., Shokurov, M.V., Yarovaya, D.A., Hein, D., 2009. Statistics of mesoscale cyclonic eddies over the Black Sea. Phys. Oceanogr. 19 (4), 211–224.
Fedorov, K.N., Ginsburg, A.I., 1989. Mushroom-like currents (vortex dipoles): one of the most widespread forms of non-stationary coherent motions in the ocean. In: Elsevier Oceanography Series 50. pp. 1–14.
Fedorov, A.M., Kubryakov, A.A., Belonenko, T.V., 2017. Long-term changes in large-scale circulation in the North Atlantic Ocean based on satellite altimetry. Sovr. Probl. DZZ Kosm. 14 (7), 225–237.
Fore, A.G., Stiles, B.W., Chau, A.H., Williams, B.A., Dunbar, R.S., Rodriguez, E., 2014. Point-wise wind retrieval and ambiguity removal improvements for the QuikSCAT climatological data set. IEEE Trans. Geosci. Remote Sens. https://doi.org/10.1109/TGRS.2012.2235843.
Garmashov, A.V., Polonsky, A.B., 2011. Wind variability in the northwestern part of the Black Sea from the offshore fixed platform observation data. Russ. Meteorol. Hydrol. 36 (12), 811–818.
Garmashov, A.V., Kubryakov, A.A., Shokurov, M.V., Stanichny, S.V., Toloknov, A.I., Korovushkin, Yu.N., 2016. Comparing satellite and meteorological data on wind velocity over the Black Sea. Izv. Atmos. Oceanic Phys. 52 (3), 309–316.
Ginzburg, A.I., Kostianoy, A.G., Krivosheya, V.G., Nezlin, N.P., Soloviev, D.M., Stanichny, S.V., Yakubenko, V.G., 2002. Mesoscale eddies and related processes in the northeastern Black Sea. J. Mar. Syst. 32 (1), 71–90.
Goryachkin, Yu.N., Kondratiev, S.I., Lisichenok, A.D., 2005. Hydrological-hydrochemical characteristics and dynamics of waters in the Kerch Strait in March 2004. In: Ecological Safety of Coastal and Shelf Zones and Complex Use of Shelf Resources. 12. pp. 108.
Grégoire, M., Lacroix, G., 2003. Exchange processes and nitrogen cycling on the shelf and continental slope of the Black Sea basin. Glob. Biogeochem. Cycles 17 (2).
Grigoriev, A.V., Petrenko, L.A., 1999. Black Sea as a factor of influence on atmospheric processes in the region. In: Ecological Safety of Coastal and Shelf Zones and Complex Use of Shelf Resources. 1. pp. 17.
Grishin, G., Bayankina, T., Kalinin, E., Lundberg, M., 1991. Evolution of southern cyclones in the Black-Sea and the Ukraine, from satellite and ground observations. Sov. J. Remote. Sens. 9 (3), 484–493.
Gusev, A.M., 1959. The Novorossiysk Bora. Akad. Nauk SSSR, Moscow (in Russian).
Ilyin, Y.P., Lemeshko, E.M., Stanichny, S.V., Soloviev, D.M., 1999. Satellite observations of similar circulation features in semi-enclosed basins of the Eastern Mediterranean with respect to marine ecosystems investigations. In: MalanotteRizzoli, P., Eremeev, V.N. (Eds.), The Eastern Mediterranean as a Laboratory Basin for the Assessment of Contrasting Ecosystems. Kluwer Academic Publishers, The Netherlands, pp. 417–422.
Ilyin, Y.P., Repetin, L.N., Belokopytov, V.N., Goryachkin, Y.N., Dyakov, N.N., Kubryakov, A.A., Stanichny, S.V., 2012. Meteorological conditions of the seas of Ukraine. In: Black Sea. 2. pp. 421 (In Russian).
Ivanov, V.A., Belokopytov, V.N., 2013. Oceanography of the Black Sea. ECOSY-Gidrofizika.
Kara, A.B., Hurlburt, H.E., Wallcraft, A.J., Bourassa, M.A., 2005. Black Sea mixed layer sensitivity to various wind and thermal forcing products on climatological time scales. J. Clim. 18 (24), 5266–5293.
Kazmin, A.S., Zatsepin, A.G., 2007. Long-term variability of surface temperature in the Black Sea, and its connection with the large-scale atmospheric forcing. J. Mar. Syst. 68 (1–2), 293–301.
Korotaev, G.K., 2001. On the source of the seasonal course of the Black Sea circulation. Morsk. Gidrofiz. Zh. 6, 14–20.
Korotaev, G.K., Saenko, O.A., Koblinsky, C.J., 2001. Satellite altimetry observations of the Black Sea level. J. Geophys. Res. Oceans 106 (C1), 917–933.
Kosyan, R.D., Goryachkin, Y.N., Krylenko, V.V., Dolotov, V.V., Krylenko, M.V., Godin, E.A., 2012. Crimea and Caucasus accumulative coasts dynamics estimation using satellite pictures. Turk. J. Fish. Aquat. Sci. 12 (5), 385–390.
Krivosheya, V.G., Moskalenko, L.V., Melnikov, V.A., Skirta, A.Y., 2012. Effects of the wind and thermal conditions variability on the structure and dynamics of the seawater in the Northeastern Black Sea. Oceanology 52 (4), 453–466.
Kubryakov, A.A., Stanichny, S.V., 2015a. Seasonal and interannual variability of the Black Sea eddies and its dependence on characteristics of the large-scale circulation. Deep-Sea Res. I Oceanogr. Res. Pap. 97, 80–91.
Kubryakov, A.A., Stanichny, S.V., 2015b. Dynamics of Batumi anticyclone from the satellite measurements. Phys. Oceanogr. (2), 59–68.

Kubryakov, A.A., Shokurov, M.V., Stanichny, S.V., Anisimov, A.E., 2015. Land–sea temperature contrasts in the black sea region and their impact on surface wind variability. Izv. Atmos. Oceanic Phys. 51 (4), 444–453.
Kubryakov, A.A., Stanichny, S.V., Zatsepin, A.G., Kremenetskiy, V.V., 2016. Long-term variations of the Black Sea dynamics and their impact on the marine ecosystem. J. Mar. Syst. 163, 80–94.
Kubryakov, A.A., Stanichny, S.V., Volkov, D.L., 2017. Quantifying the impact of basin dynamics on the regional sea level rise in the Black Sea. Ocean Sci. 13 (3), 443.
Kubryakov, A.A., Stanichny, S.V., Zatsepin, A.G., 2018. Interannual variability of Danube waters propagation in summer period of 1992–2015 and its influence on the Black Sea ecosystem. J. Mar. Syst. 179, 10–30.
Kubryakov, A.A., Zatsepin, A.G., Stanichny, S.V., 2019. Anomalous summer-autumn phytoplankton bloom in the Black Sea driven by several strong wind events. J. Mar. Syst (accepted, S0924-7963(18)30088-5).
Lefevre, R.J., Nielsen-Gammon, J.W., 1995. An objective climatology of mobile troughs in the Northern Hemisphere. Tellus ASCAT 47 (5), 638–655.
Monin, A.S., Obukhov, A.M., 1954. Basic laws of turbulent mixing in the surface layer of the atmosphere. Contrib. Geophys. Inst. Acad. Sci. USSR 151 (163), e187.
Moore, G.W.K., Renfrew, I.A., 2005. Tip jets and barrier winds: ASCAT QuikSCAT climatology of high wind speed events around Greenland. J. Clim. 18 (18), 3713–3725.
Oguz, T., Latun, V.S., Latif, M.A., Vladimirov, V.V., Sur, H.I., Markov, A.A., ... Ünlüata, Ü., 1993. Circulation in the surface and intermediate layers of the Black Sea. Deep-Sea Res. I Oceanogr. Res. Pap. 40 (8), 1597–1612.
Oguz, T., Deshpande, A.G., Malanotte-Rizzoli, P., 2002. The role of mesoscale processes controlling biological variability in the Black Sea coastal waters: inferences from SeaWIFS-derived surface chlorophyll field. Cont. Shelf Res. 22 (10), 1477–1492.
Onea, F., Rusu, E., 2014. Wind energy assessments along the Black Sea basin. Meteorol. Appl. 21 (2), 316–329.
Panagiotopoulos, F., Shahgedanova, M., Hannachi, A., Stephenson, D.B., 2005. Observed trends and teleconnections of the Siberian high: ASCAT recently declining center of action. J. Clim. 18 (9), 1411–1422.
Pickart, R.S., Spall, M.A., Ribergaard, M.H., Moore, G.W.K., Milliff, R.F., 2003. Deep convection in the Irminger Sea forced by the Greenland tip jet. Nature 424 (6945), 152.
Pustovoitenko, V.V., Malinovsky, V.V., 1998. Some peculiarities of processing information of the satellite radar sensor station side survey "Och-1". Morsk. Gidrofiz. Zh. 3, 70.
Repetin, L.N., Belokopytov, V.N., 2008. Wind regime on the coast and shelf zone of the northeastern Black Sea. Naukovi Pratsi Ukrainskogo Naukovo-Doslidnogo Gidrometeorologichnogo Instytutu 257, 89–105.
Repetin, L.N., Belokopytov, V.N., 2009. The wind regime of the north-western part of the Black Sea and its climatic change. In: Ecological Safety of Coastal and Shelf Zones and Complex Use of Shelf Resources. 17. pp. 225–243.
Risien, C.M., Chelton, D.B., 2008. ASCAT global climatology of surface wind and wind stress fields from eight years of QuikSCAT scatterometer data. J. Phys. Oceanogr. 38 (11), 2379–2413.
Shapiro, G.I., Stanichny, S.V., Stanychna, R.R., 2010. Anatomy of shelf–deep sea exchanges by a mesoscale eddy in the North West Black Sea as derived from remotely sensed data. Remote Sens. Environ. 114 (4), 867–875.
Shcherbak, S.S., Lavrova, O.Y., Mityagina, M.I., Bocharova, T.Y., Krovotyntsev, V.A., Ostrovskii, A.G., 2008. Multisensor satellite monitoring of seawater state and oil pollution in the northeastern coastal zone of the Black Sea. Int. J. Remote Sens. 29 (21), 6331–6345.
Shokurov, M.V., 2011. Numerical simulation of atmospheric circulation over the Black Sea. Ekol. Bezop. Pribrezhn. Shel'fovoi Zon Kompleksn. Ispol'z. Resur. Shel'fa 2 (25), 91–113.
Shokurov, M.V., 2012. Numerical modeling of catastrophic weather phenomena in the Black Sea region. In: Ecological Safety of Coastal and Shelf Zones and Complex Use of Shelf Resources. 26(2). pp. 301–320 (in Russian).
Shokurov, M.V., Shokurova, I.G., 2017. Wind stress curl over the Black Sea under different wind regimes. Phys. Oceanogr. 6.
Hydrometeorology and hydrochemistry of the USSR seas. In: Simonov, Altman (Eds.), The Black Sea. vol. IV Gidrometeoizdat (430 pp.).
Sorokina, A., 1974. Reference Book on the Black Sea Climate. Gidrometeoizdat, Moscow (406 pp.).
Stanev, E.V., 1990. On the mechanisms of the Black Sea circulation. Earth-Sci. Rev. 28, 285–319.
Stanev, E.V., Le Traon, P.Y., Peneva, E.L., 2000. Sea level variations and their dependency on meteorological and hydrological forcing: analysis of altimeter and surface data for the Black Sea. J. Geophys. Res. Oceans 105 (C7), 17203–17216.
Stoffelen, A.C.M., Vries, J., Voorrips, A.C., 2001. Towards the Real-time Use of QuikSCAT Winds. Netherlands Remote Sensing Board (BCRS), Programme Bureau, Rijkswaterstaat Survey Department.
Toloknov, Yu.N., Korovushkin, A.I., Kozlov, K.G., 1998. Automated hydrometeorological system. In: Environmental Control Systems. NPTs "EKOSIGidrofizika", Sevastopol, pp. 12–17 (in Russian).
Valchev, N., Davidan, I., Belberov, Z., Palazov, A., Valcheva, N., 2010. Hindcasting and assessment of the western Black Sea wind and wave climate. J. Environ. Prot. Ecol. 11 (3), 1001–1012.
Van Vledder, G.P., Akpınar, A., 2015. Wave model predictions in the Black Sea: sensitivity to wind fields. Appl. Ocean Res. 53, 161–178.
Verhoef, A., Stoffelen, A., 2013. Validation of ASCAT coastal winds. In: Tech. Report, Version 1.5, SAF/OSI/CDOP/KNMI/TEC/RP/176, (Sponsored by EUMETSAT).
Verspeek, J.A., Stoffelen, A., Portabella, M., Bonekamp, H., Anderson, C., Figa, J., 2009. Validation and calibration of ASCAT using CMOD5.n. IEEE Trans. Geosci. Remote Sens. 48 (1), 386–395. https://doi.org/10.1109/TGRS.2009.2027896.
Yarovaya, D.A., 2016. Intense mesocyclones in the Black Sea region. Russ. Meteorol. Hydrol. 41 (8), 535–543.
Yarovaya, D.A., Efimov, V.V., 2014. Mesoscale cyclones over the Black Sea. Russ. Meteorol. Hydrol. 39 (6), 378–386.
Yarovaya, D.Y., Shokurov, M.V., 2012. Mesoscale cyclonic vortices formed over the Black Sea near the Caucasian coast. Morskoi Gidrofizicheskii Zhurnal 3.
Zamudio, L., Hurlburt, H.E., Metzger, E.J., Morey, S.L., O'Brien, J.J., Tilburg, C., Zavala-Hidalgo, J., 2006. Interannual variability of Tehuantepec eddies. J. Geophys. Res. Oceans 111 (C5).
Zatsepin, A.G., Kremenetskiy, V.V., Poyarkov, S.G., Ratner, Y.B., Stanichny, S.V., 2002. Influence of wind field on water circulation in the Black Sea. In: Complex Investigation of the Northeastern Black Sea. Nauka, Moscow, pp. 91–105.
Zatsepin, A.G., Ginzburg, A.I., Kostianoy, A.G., Kremenetskiy, V.V., Krivosheya, V.G., Stanichny, S.V., Poulain, P.M., 2003. Observations of Black Sea mesoscale eddies and associated horizontal mixing. J. Geophys. Res. Oceans 108 (C8).
Zatsepin, A.G., Denisov, E.S., Emel yanov, S.V., Kremenetskiy, V.V., Poyarkov, S.G., Stroganov, O.Y., ... Stanichny, S.V., 2005. Effect of bottom slope and wind on the near-shore current in a rotating stratified fluid: laboratory modeling for the Black Sea. Oceanology c/c of Okeanologiia 45, S13.
Zatsepin, A.G., Golenko, N.N., Korzh, A.O., Kremenetskii, V.V., Paka, V.T., Poyarkov, S.G., Stunzhas, P.A., 2007. Influence of the dynamics of currents on the hydrophysical structure of the waters and the vertical exchange in the active layer of the Black Sea. Oceanology 47 (3), 301–312.
Zatsepin, A., Kubryakov, A., Aleskerova, A., Elkin, D., Kukleva, O., 2019. Physical mechanisms of submesoscale eddies generation: evidences from laboratory modeling and satellite data in the Black Sea. Ocean Dyn. 1–14.
Zecchetto, S., De Biasio, F., 2007. Sea surface winds over the Mediterranean basin from satellite data (2000–04): meso-and local-scale features on annual and seasonal time scales. J. Appl. Meteorol. Climatol. 46 (6), 814–827.
Zhou, F., Shapiro, G., Wobus, F., 2014. Cross-shelf exchange in the northwestern Black Sea. J. Geophys. Res. Oceans 119 (4), 2143–2164.